

Shape Morphometry Using Riemannian Geometry with
Applications in Medical Imaging

TSANG, Man Ho

A Thesis Submitted in Partial Fulfillment
of the Requirements for the Degree of
Master of Philosophy
in
Mathematics
The Chinese University of Hong Kong
August 2013

Table of Contents

Table of Contents	i
Abstract	iii
Acknowledgements	iv
Introduction	1
0.1 Previous Works	4
1 Mathematical Backgrounds	7
1.1 Riemannian Manifold	7
1.2 Conformal Mapping	10
1.3 Quasi-conformal Mapping	15
1.4 Laplace-Beltrami operator	18
2 Quasi-conformal Mapping For Medical Surface Registration	24
2.1 Introduction	24
2.2 Quasi-conformal (QC) iteration	24
2.2.1 Computing Beltrami coefficient	25
2.2.2 Main algorithm	25
2.3 Experimental result and conclusion	29
2.3.1 Brainstem	29
2.3.2 Teeth	34
2.3.3 Conclusion	39
3 Feature Extraction of Anatomic Structure	41
3.1 Introduction	41
3.2 Chan-Vese segmentation	42
3.3 Proposed algorithm	44

3.4 Results and conclusion	47
4 Conclusion	55
Bibliography	57

Abstract

Shape morphometry is the quantitative analysis on the shape of geometric subjects, usually human organs and other organism. As a field of mathematics, it consists of surface reconstruction, surface processing, landmark extraction, surface registration and shape analysis. In this thesis, we will focus on surface registration and landmark extraction by using Riemannian geometry. A registration between surfaces is needed for the one-one correspondence between them so that the local shape difference between specimens can be analysed. Conformal maps have been widely used as the registration between surfaces. As conformal maps preserve angles, the local geometry can be preserved well. However, the existence of a conformal map is not guaranteed when landmark are required to be matched. Therefore, the quasi-conformal map, which is a generalization of conformal maps, are usually used as a landmark-based registration. We propose to apply the Quasi-conformal (QC) iteration developed in [15] to find the landmark-matching registration between medical images. The Teichmüller extremal maps (T-maps), which is the quasi-conformal map minimizing the maximal conformality distortion among all diffeomorphism between the surfaces, can be effectively computed by the QC iteration. For a landmark-based registration, the landmark points, which are points of correspondence on each specimen that match between and within populations, are needed to be extracted before the registration. Automatic or semi-automatic algorithm is needed for large-scale experiment. In this thesis, we will apply the QC algorithm to find registrations between some human organs, and develop a semi-automatic landmark extraction algorithm on brainstem surfaces.

摘要:

形態計量學是幾何形狀的定量分析，對象通常是人體器官和其他生命體。作為一個數學領域，它包含表面重建，表面處理，地標提取，表面配準和形狀分析。在這篇論文中，我們將專注於通過使用形幾何來進行表面配準和地標提取。為分析樣本之間的局部形狀差異，我們需要表面之間的配準作為一一對應。共形映射已被廣泛用作表面之間的配準，由於共形映射保存角度，局部的幾何形狀可以保存完好。然而，當地標須配對時，我們不能保證一個形映射的存在。因此，擬共形映射，共形映射的一般化，會被用作於地標配對配準上。我們建議使用一個名為 **Quasi-conformal (QC)** 的疊代法 [15]，來用於醫療圖像之間的地標配對配準。QC 疊代法可以有效地計算出 **Teichmüller Extremal 映射 (T-map)**，此映射在所有配對地標的擬共形映射中擁有最小的共形失真。地標點是每個樣本和種群之間的對應點，他們都需要在基於地標的配準前提取。在進行大規模的實驗時，都需要自動或半自動的地標提取算法。在這篇論文中，我們將運用 QC 疊代法找到一些人體器官之間的配準，並開發一種腦幹表面上的半自動地標提取算法。

Acknowledgements

I would like to thank Professor **Lui Lok Ming Ronald**, my supervisor, for his guidance and support during this research. Lam Ka Chun and Wen Chengfeng also helped a lot on the research. I would also like to thank Lee Yin Tat for his brilliant suggestions. Without them, this thesis would be a dream.

Next, I would also like to thank Leung Wing Tak, Chow Yat Tin , Yu Tang Fei and Wang Shiping for their many helpful suggestion throughout my graduate studies. Many thanks are also due to Choi Chi Po, Ng Tsz Ching, Cho Chi Lam, Yuen Man Chun, Mak Tsz Fan, Lam Chi Yeung, Chan Chi Ming, Lam Wai Kit, Lam Yi Chun, Lin Jessey, Wong Chun Yin, Mak Tsz Kin and many others for their many discussions.

Last but not least, I would also like to thank my parents for their endless support and love throughout my life.

Tsang Man Ho

June 7, 2013

Introduction

In the field of biology and physiology, shape morphometry is the quantitative analysis on the shape of geometric subjects, usually human organs and other organism. It includes the statistical analysis of shape variation among a species and the analysis of shape change as a result of growth, experimental treatment, evolution or diseases [25]. Traditionally, the lengths, widths, masses, angles, ratios and areas are often analysed. Landmark points are taken from the specimen and the distance between specific landmark points are measured as data. Statistical analysis, such as the principal component analysis (PCA) are done on the data collected. The drawback of the traditional approach is that the length collected are usually highly correlated. Very little information about the shape and size is collected [23]. In modern morphometry, the 2- or 3-dimensional coordinates of the landmark and semilandmark points on the specimen are collected as data. The spatial information and the geometry of the specimen can then be analysed [29].

However, shape morphometry is a much wider topic in mathematics. It consists of surface reconstruction (reconstruction of a surface from a set of point cloud taken from medical images, such as MRIs), surface processing (including denoising, smoothing, inpainting, mesh reconstruction, etc.), landmark extraction, surface registration (finding the one-one correspondence between surfaces) and shape analysis (statistical

analysis on the shape difference between surfaces, usually by comparing a shape index). In this thesis, we will focus on surface registration and landmark extraction by using Riemannian geometry.

A registration is needed for the one-one correspondence between different specimens. The registration methods can be divided into two types: landmark-based and non-landmark-based. A non-landmark-based registration usually utilize geometric structures, such as the curvature of a surface, as the reference for the registration. An energy functional measuring the curvature mismatch, for example, can be constructed for a surface registration problem and the diffeomorphism between the surfaces that minimizes the energy functional can be used as the registration. On the other hand, a landmark-based registration will map landmark points of a specimen to the corresponding landmark points of another, or map the landmark points of different specimens to the same spots on the parametric domain. An energy functional measuring the landmark mismatch, for example, can be constructed for a landmark-matching registration problem and the diffeomorphism between the surfaces that minimizes the energy functional will be the landmark-matching registration. With the registration, statistical analysis can be performed. An overview of different registration method for medical images can be found in [22].

Conformal maps have been widely used for registration between two surfaces [11, 8, 27, 9]. As conformal maps preserve angles, the local geometry can be preserved well. Given two simply-connected surfaces, there exists a unique conformal map up to a Möbius transform. However, if landmark matching are required, a conformal map may not exist. Therefore, the quasi-conformal map, which is a generalization of conformal maps, are usually used as a landmark-based registration between surfaces.

We propose to apply the Quasi-conformal (QC) iteration developed in [15] to find the landmark-matching registration between medical images. The Teichmüller extremal maps (T-maps), which is the quasi-conformal map minimizing the maximal conformality distortion among all diffeomorphism between the surfaces, can be effectively computed by the QC iteration.

For a landmark-based registration, the landmark points are needed to be extracted before the registration. Landmarks are points of correspondence on each specimen that match between and within populations. They are biologically homologous anatomical loci recognizable on all specimens in the study. Landmarks can be defined both locally and globally, either anatomically or geometrically. Locally defined landmark includes the intersection of different components of an organism and the local minima and maxima of curvature of a surface. Globally defined landmarks are usually the points that are furthest away, such as the two tips of a structure. Semilandmarks are points along a curve, usually forming a curve joining the landmarks. They are usually ridges, valleys or geodesics on a surface [1] [4] [28]. For simplicity, we will call both the landmarks and semilandmark as landmarks in this paper.

Landmark points can be extracted manually. It is accurate, but the process will be very slow for a large-scale morphometry. Therefore developing an automatic or semi-automatic method for landmark extraction is important. Automatic landmark extraction is fast, but we have not much control on landmark extracted. The target landmarks may not be extracted while the extracted curves may not be landmarks. Therefore, we propose a semi-automatic landmark extraction algorithm, which requires background knowledge on the specific surface to assign different parameters

for each landmark. For each landmark, some times are needed to spend on assigning the parameters, but the computation will be automatic and it can deal with any number of specimens.

In this thesis, we will apply the QC iteration developed in [15] to find registrations between some human organs, and develop a semi-automatic landmark extraction algorithm on brainstem surfaces.

0.1 Previous Works

Surface registration, which aims at finding meaningful one-one correspondence between surfaces, has been studied extensively by different groups. Conformal surface registration is widely used [11, 8, 27, 9]. For example, Hurdal et al. [11] proposed to compute the conformal parametrization using circle packing and applied it to human brain surface registration. Gu et al. [8, 27, 9] proposed to compute the conformal parametrization of Riemann surfaces for registration using harmonic energy minimization and holomorphic 1-forms. Using conformal parametrization for surface registrations is advantageous as they preserve local geometry well.

Sometimes, the deformations between surfaces may not be conformal. For example, the normal growth of human brains may be conformal, but in case of some diseases, the growth may be abnormal and the deformation may not be conformal. There may not certain amounts of conformality distortion. Therefore, quasi-conformal mappings are proposed as the smooth one-one correspondence with bounded conformality distortion. Lui et al. [19] proposed to compute the quasi-conformal maps between hippocampal surfaces which minimize curvature mismatch. The Beltrami Holomorphic flow is used to obtain the optimal Beltrami coefficient associated to

the registration [20]. Wei et al. [30] proposed to compute quasi-conformal mapping for feature matching face registration. The Beltrami coefficient associated to the landmark matching parametrization is approximated. However, exact landmark matching and bijectivity of the mapping cannot be guaranteed, especially when the deformations is very large. In order to find the quasi-conformal maps from the associated Beltrami coefficient effectively, the Quasi-Yamabe method is introduced, which applies the curvature flow method to compute the quasi-conformal maps [31]. The algorithm can deal with surfaces with general topologies. The Linear Beltrami Solver (LBS) is introduced in [15]. It can compute the quasi-conformal mapping from its associated Beltrami coefficient more effectively.

Landmark-based diffeomorphisms are often used to compute, or adjust, cortical surface parameterizations [7, 13]. For example, Glaunes et al. [7] proposed to generate large deformation diffeomorphisms of the sphere onto itself, given the displacements of a finite set of template landmarks. Leow et al. [13] proposed a level-set based approach to match different types of features, including points and 2D or 3D curves represented as implicit functions. These methods provide good registrations when the corresponding landmark points on the surfaces can be labeled in advance. On surfaces without well-defined landmarks, some authors have proposed driving features into correspondence based on shape information. Lyttelton et al. [21] computed surface parameterizations that match surface curvature. Fischl et al. [5] improved the alignment of cortical folding patterns by minimizing the mean squared difference between the average convexity across a set of subjects and that of the individual. Lord et al. [14] matched surfaces by minimizing the deviation from isometry. Wang et al. [26, 18] proposed to compute the optimized conformal parameterizations of

brain surfaces by minimizing a compounded energy. The features of the surfaces are aligned, but the landmarks are not exactly matched. Besides, the resultant mapping may not be a diffeomorphism when the number of landmarks is large. Lui et al. [16, 17] proposed to use vector fields to represent surface maps. The registrations are reconstructed by the integral flow equations. A shape-based landmark matching harmonic maps is obtained by looking for the best vector fields minimizing a shape energy. The use of vector fields makes optimization easier, although it cannot describe all surface maps. Landmarks are exactly matched by the resultant mapping. Zhang et al. [32] parameterized brainstem surface conformally onto the quadrilaterally-faced hexahedron by discrete Ricci flow method. Landmarks are exactly matched but the mapping is not continuous at the landmarks. Lui et al. [15] proposed to use the Teichmüller extremal maps (T-map) as the one-one correspondence between surfaces while matching landmarks. T-map is a class of quasi-conformal maps, and the T-map with minimal conformality distortion can be found iteratively by an iterative scheme called the Quasi-conformal (QC) iteration. Large number of landmark constrains can be enforced, and the bijectivity is ensured even with large deformation.

Chapter 1

Mathematical Backgrounds

1.1 Riemannian Manifold

Definition 1.1.1. A *manifold* is a topological space S covered by a set of open sets $\{U_\alpha\}$. A homeomorphism $\phi_\alpha : U_\alpha \rightarrow \mathbb{R}^n$ maps U_α to the Euclidean space \mathbb{R}^n . (U_α, ϕ_α) is called a *coordinate chart* of M , the set of all charts $\{(U_\alpha, \phi_\alpha)\}$ form the *atlas* of M . Suppose $U_\alpha \cap U_\beta \neq \emptyset$. Then

$$\phi_{\alpha\beta} = \phi_\beta \circ \phi_\alpha^{-1} : \phi_\alpha(U_\alpha \cap U_\beta) \rightarrow \phi_\beta(U_\alpha \cap U_\beta)$$

is called a *transition map*.

If all transition functions $\phi_{\alpha\beta}$ are smooth, then the manifold is called a *differential manifold*, or a *smooth manifold*. The atlas is a *differential atlas*. The maximal differential atlas is called a *differential structure*.

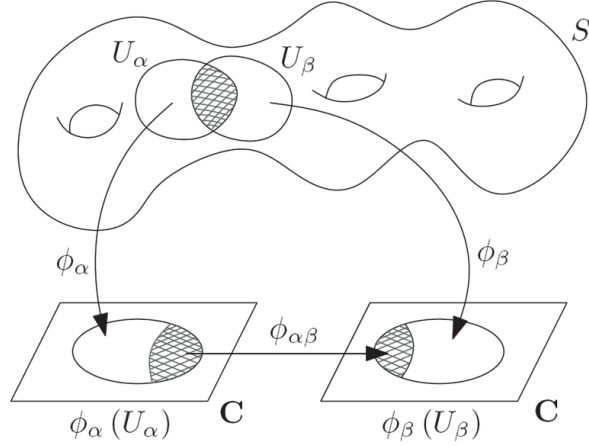
Suppose M is a smooth manifold embedded in \mathbb{R}^n , a curve on the manifold is a map

$$\gamma : (-\varepsilon, \varepsilon) \rightarrow M.$$

Definition 1.1.2. A vector $\mathbf{v} \in \mathbb{R}^{n+1}$ is said to be *tangent* to $M \subset \mathbb{R}^{n+1}$ at a point $p \in M$, if there exists a smooth curve γ with $\gamma(0) = p$ and $\gamma'(0) = \mathbf{v}$.

The set $T_p M$ of all the vectors tangent to the manifold $M \subset \mathbb{R}^{n+1}$ at the point p is a vector space. It is called the *tangent space*. A tangent vector can be abstractly defined without embedding as follows.

Definition 1.1.3. A tangent vector is represented by elements of \mathbb{R}^n for each coordinate chart transforming via differentials of a coordinate change at the reference



point.

Mathematically, a tangent vector ξ at the point p is an n -tuple $(\xi^1, \xi^2, \dots, \xi^n)$ of real numbers associate to a coordinate chart (x^1, x^2, \dots, x^n) at p , such that if $(\tilde{\xi}^1, \tilde{\xi}^2, \dots, \tilde{\xi}^n)$ is associated with another coordinate system $(\tilde{x}^1, \tilde{x}^2, \dots, \tilde{x}^n)$, then it satisfies the transition rule

$$\tilde{\xi}^i = \sum_{j=1}^n \frac{\partial \tilde{x}^i}{\partial x^j}(p) \xi^j.$$

A *smooth vector field* ξ assigns a tangent vector for each point of M , it has a local representation

$$\xi(x^1, x^2, \dots, x^n) = \sum_{i=1}^n \xi_i(x^1, x^2, \dots, x^n) \frac{\partial}{\partial x_i}.$$

where $\left\{ \frac{\partial}{\partial x_i} \right\}$ represents the vector fields associate with the iso-parametric curves of M . They form a basis of all vector field.

Suppose $\phi : M \rightarrow N$ is a differentiable map from M to N , $\gamma : (-\varepsilon, \varepsilon) \rightarrow M$ is a curve, $\gamma(0) = p$, $\gamma'(0) = \mathbf{v} \in T_p M$. Then $\phi \circ \gamma$ is a curve on N , $\phi \circ \gamma(0) = \phi(p)$. We define the tangent vector

$$\phi_*(\mathbf{v}) = (\phi \circ \gamma)'(0) \in T_{\phi(p)} N,$$

as the *push-forward* tangent vector of \mathbf{v} induced by ϕ .

Definition 1.1.4. The tangent space $T_p M$ is an n -dimensional vector space, its dual space $T_p^* M$ is called the *cotangent space* of M at p . Suppose $\omega \in T_p^* M$. Then

$\omega : T_p M \longrightarrow \mathbb{R}$ is a linear function defined on $T_p M$, ω is called a *differential 1-form* at p .

Similarly, we can define the differential 1-form field, it has the local representation

$$\omega(x^1, x^2, \dots, x^n) = \sum_{i=1}^n \omega_i(x^1, x^2, \dots, x^n) dx_i$$

where $\{dx_i\}$ are the dual differential 1-forms to $\left\{\frac{\partial}{\partial x_j}\right\}$, such that

$$dx_i \left(\frac{\partial}{\partial x_j} \right) = \delta_{ij}$$

where

$$\delta_{ij} = \begin{cases} 1, & i = j \\ 0, & i \neq j \end{cases}.$$

Definition 1.1.5. A tensor Θ of type (n, m) on a manifold M is a correspondence that associates to each point $p \in M$ a multi-linear map

$$\Theta_p : T_p M \times T_p M \times \dots \times T_p M \times T_p^* M \times \dots \times T_p^* M \longrightarrow \mathbb{R},$$

where the tangent space $T_p M$ appears m times and the cotangent space $T_p^* M$ appears n times.

Definition 1.1.6. A *Riemannian manifold* (M, g) is a smooth manifold M equipped with a *Riemannian metric* g . A Riemannian metric on M is a family of positive definite inner products $g_p : T_p M \times T_p M \longrightarrow \mathbb{R}$, $p \in M$, such that for all differentiable vector fields X, Y on M , $p \mapsto g_p(X(p), Y(p))$ defines a smooth function $M \longrightarrow \mathbb{R}$.

The Riemannian metric is a symmetric $(0, 2)$ -tensor that is positive definite, i.e. $g(X, X) > 0$ for all $X \neq 0$. Under the local coordinate system $\left\{\frac{\partial}{\partial x^j}\right\}$, the metric tensor can be expressed locally at $p \in M$ as

$$g_{ij}(p) = g_p \left(\left(\frac{\partial}{\partial x^i} \right), \left(\frac{\partial}{\partial x^j} \right) \right).$$

Equivalently, the metric tensor can be written in terms of the dual basis $\{dx^1, \dots, dx^n\}$ of the cotangent bundle as

$$g = \sum_{i,j} g_{ij} dx^i \otimes dx^j.$$

Definition 1.1.7. Suppose $\phi : M \longrightarrow N$ is a differential map and (N, g) is a Riemannian manifold. The pullback metric ϕ^*g is a $(0, 2)$ -tensor defined as

$$\phi^*g(v, w) = g(\phi_*(v), \phi_*(w))$$

for $v, w \in T_pM$, where $\phi_*(v)$ is the push-forward of v by ϕ . [10]

1.2 Conformal Mapping

Definition 1.2.1. Let $u : D \rightarrow \mathbb{R}$ be a real-valued function defined on a domain $D \subset \mathbb{C}$. If $u \in C^2(D)$ and

$$\Delta u(z) = \frac{\partial^2 u(z)}{\partial x^2} + \frac{\partial^2 u(z)}{\partial y^2} = 0$$

for all $z \in D$, then u is called a *harmonic function*. Δ is called the *Laplace operator*.

We denote

$$dz = dx + idy$$

$$d\bar{z} = dx - idy$$

$$\frac{\partial}{\partial z} = \frac{1}{2} \left(\frac{\partial}{\partial x} - i \frac{\partial}{\partial y} \right)$$

$$\frac{\partial}{\partial \bar{z}} = \frac{1}{2} \left(\frac{\partial}{\partial x} + i \frac{\partial}{\partial y} \right)$$

The Laplace operator can be expressed as

$$\Delta = 4 \frac{\partial^2}{\partial z \partial \bar{z}}$$

Definition 1.2.2. A function $f : \mathbb{C} \rightarrow \mathbb{C}$, $f(x + iy) = u + iv$ is called a *holomorphic function* if it satisfies the *Cauchy-Riemann equation*:

$$\begin{aligned} \frac{\partial u}{\partial x} &= \frac{\partial v}{\partial y} \\ \frac{\partial u}{\partial y} &= -\frac{\partial v}{\partial x} \end{aligned}$$

As a consequence, if a function f is holomorphic, then

$$\frac{\partial f}{\partial \bar{z}} = 0$$

and both u and v are harmonic.

A function $f : D \rightarrow \mathbb{C}$ is called *biholomorphic* if it is bijective and its inverse f^{-1} is holomorphic.

Definition 1.2.3. A *Riemann Surface* represents a two-dimensional manifold M with an atlas $\{(U_\alpha, z_\alpha)\}$, such that

1. $\{U_\alpha\}$ is an open covering, i.e. $M \subset \bigcup U_\alpha$,
2. $z_\alpha : U_\alpha \rightarrow \mathbb{C}$ is a homeomorphism from an open set $U_\alpha \subset M$ to an open set $z_\alpha(U_\alpha) \subset \mathbb{C}$, and
3. If $U_\alpha \cap U_\beta \neq \emptyset$, then

$$z_\beta \circ z_\alpha^{-1} : z_\alpha(U_\alpha \cap U_\beta) \rightarrow z_\beta(U_\alpha \cap U_\beta)$$

is biholomorphic.

Definition 1.2.4. Let M and \tilde{M} be two Riemann surfaces. A mapping $f : M \rightarrow \tilde{M}$ is called a *conformal mapping*, if for any $p \in M$, $\tilde{p} = f(p) \in \tilde{M}$, and for any local parameter charts (U, ϕ) and $(\tilde{U}, \tilde{\phi})$, $z = \phi(p)$, $\tilde{z} = \tilde{\phi}(\tilde{p})$, then

$$\tilde{z} = \tilde{\phi} \circ f \circ \phi^{-1}(z)$$

is holomorphic in U .

Theorem 1.2.1. Let $f : \mathbb{C} \rightarrow \mathbb{C}$ be a holomorphic function and $w = f(z)$. Then

$$\begin{aligned} dw &= \frac{\partial f(z)}{\partial z} dz + \frac{\partial f(z)}{\partial \bar{z}} d\bar{z} \\ &= \frac{\partial f(z)}{\partial z} dz \end{aligned}$$

as $\frac{\partial f(z)}{\partial \bar{z}} = 0$. Therefore

$$dw^2 = dw d\bar{w} = \left| \frac{\partial f(z)}{\partial z} \right|^2 dz d\bar{z} = \lambda (dz^2)$$

which implies that the pull back metric dw^2 induced by f is equal to the original metric up to a scaling factor $\lambda = \left| \frac{\partial f(z)}{\partial z} \right|^2$, which is also called the conformal factor, and thus a holomorphic function between planar domains preserves angles. Similarly, conformal mappings between Riemann surfaces with metrics also preserve angles.

Theorem 1.2.2. (Riemann Mapping Theorem) Let $D \subset \mathbb{C}$ be a simply-connected domain in the complex plane, with an interior point $z_0 \in D$. There exists a unique conformal mapping ϕ from domain D to the unit disk Δ , such that $\phi(z_0) = 0$ and $\phi'(z_0) > 0$

There are several ways to find the conformal map, which will be briefly explained below:

For a topological disk D , a conformal map $u : D \rightarrow \Omega \subset \mathbb{R}^2$ can be computed by minimizing the harmonic energy.

Definition 1.2.5. (Harmonic Energy) Let (M, g) , (N, h) be Riemann surfaces with metrics g and h respectively, and $u : M \rightarrow N$ is continuously differentiable. We denote the metrics as

$$ds_M^2 = \sum g_{\alpha\beta}(x) dx^\alpha dx^\beta, \quad ds_N^2 = \sum h_{ij}(u(x)) du^i du^j.$$

The pull-back metric of h , $u^*(ds_N^2)$ is defined as

$$u^*(ds_N^2) = \sum_{\alpha,\beta} \left(\sum_{i,j} h_{ij}(u(x)) \frac{\partial u^i}{\partial x^\alpha} \frac{\partial u^j}{\partial x^\beta} \right) dx^\alpha dx^\beta.$$

The trace of the pull-back metric is called the *energy density*. It can be represented in the local coordinate system as

$$|du|^2 = Tr_g(u^*h) = \sum_{i,j,\alpha,\beta} g^{\alpha\beta} h_{ij} \frac{\partial u^i}{\partial x^\alpha} \frac{\partial u^j}{\partial x^\beta}.$$

where $\sum_j g^{ij} g_{jk} = \delta_{ik}$.

The *harmonic energy* is defined as

$$E(u) = \int_M |du|^2 dV_M$$

where $dV_M = \sqrt{\det g} dx$ is the area element of M . The critical points of E in the space of maps are called the *harmonic maps*.

If the target surface N is embedded in \mathbb{R}^3 and h is the Euclidean metric, the harmonic energy can be simplified as

$$E(u) = \sum_{i=1}^3 \int_M |\nabla u^i|^2 dV_M.$$

Definition 1.2.6. (Harmonic Map Equation) The Euler-Lagrange equation of the harmonic energy is called the *Harmonic Map Equation*. It can be expressed in the local coordinates on N as

$$\Delta u^i + \sum_{\alpha, \beta, j, k} g^{\alpha\beta} \Gamma_{jk}^i(u(x)) \frac{\partial u^j}{\partial x^\alpha} \frac{\partial u^k}{\partial x^\beta}, \quad i = 1, 2$$

where Γ_{jk}^i is the Christoffel symbols of N .

By solving the harmonic map equation, a harmonic map can be found.

Theorem 1.2.3. (Radó's Theorem) Assume $\Omega \subset \mathbb{R}^2$ is a convex domain with a smooth boundary $\partial\Omega$ and D is a topological disk with a Riemannian metric g . Given any homeomorphism $\phi : \mathbb{S}^1 \rightarrow \partial\Omega$, there exists a unique harmonic map $u : D \rightarrow \Omega$, such that $u = \phi$ on $\partial D = \mathbb{S}^1$ and u is a diffeomorphism.

A conformal map can be computed by minimizing the harmonic energy E over all orientation preserving diffeomorphism from D to Ω . Please refer to [8] for the details of the algorithm.

For a Riemann surface with genus ≥ 1 , a conformal map can be found by the holomorphic 1-form.

Definition 1.2.7. Let M be a Riemann surface with conformal atlas $\{(U_\alpha, \phi_\alpha)\}$. For each local coordinate $z_\alpha = \phi_\alpha(p)$, two smooth complex functions f_α and g_α are assigned,

$$f_\alpha dz_\alpha + g_\alpha d\bar{z}_\alpha$$

is a *complex differential 1-form* if it is invariant under coordinate changes, i.e. if $U_\alpha \cap U_\beta \neq \emptyset$, then

$$f_\alpha dz_\alpha + g_\alpha d\bar{z}_\alpha = f_\beta dz_\beta + g_\beta d\bar{z}_\beta$$

where $z_\alpha = \phi_\alpha \circ \phi_\beta^{-1}(z_\beta)$.

Definition 1.2.8. (Holomorphic 1-form) Suppose M is a Riemann surface with conformal atlas and ω is a complex differential 1-form. If on every local coordinate, ω has the representation

$$\omega = f dz,$$

where f is a holomorphic function, then ω is called a *holomorphic 1-form*. For a genus g closed surface, all holomorphic 1-forms form a $2g$ real dimensional linear space.

A point $p \in M$ is called a *zero point* of a holomorphic 1-form ω if for any local parametric representation $\omega = f(u_\alpha) dz_\alpha$, $f|_p = 0$. According to the Riemann-Roch theorem, there are, in general, $2g - 2$ zero points for a holomorphic 1-form on a surface of genus g .

A holomorphic 1-form ω can be visualized by a texture map $f : M \rightarrow \mathbb{C}$, which can be computed by integrating the holomorphic 1-form on the local parametric domain. A curve that is mapped to a horizontal line on the complex plane by f is called a *horizontal trajectory*, while a curve that is mapped to a vertical line is called a *vertical trajectory*. The horizontal and vertical trajectories that connect the zero points or a zero point and the boundary is called *critical trajectories*, which segment the surfaces into patches that are either topological disks or topological cylinders. A conformal mapping can then be easily found. Please refer to [27, 9] for the details of the algorithm.

Ricci flow is also a widely-used method for conformal mapping, which deforms the Riemannian metric of a surface conformally by its curvature.

Definition 1.2.9. (Ricci Flow) Suppose M is a smooth surface with a Riemannian metric $\mathbf{g} = (g_{ij})$. The Ricci flow deforms the metric $\mathbf{g}(t)$ conformally according to the Gaussian curvature $K(t)$ by

$$\frac{\partial g_{ij}(t)}{\partial t} = -2K(t) g_{ij}(t)$$

If the Riemannian metric is represented in the form $\mathbf{g}(t) = e^{2u(t)} \mathbf{g}(0)$, then the Ricci flow can be written as

$$\frac{\partial u(t)}{\partial t} = -2K(t).$$

It can be modified to

$$\frac{\partial u}{\partial t} = -2(\bar{K} - K)$$

so that the resultant metric will have the target curvature \bar{K} .

The algorithm for discrete Ricci flow is detailed in [3, 12].

1.3 Quasi-conformal Mapping

Definition 1.3.1. A diffeomorphism $f : D_1 \rightarrow D_2$ is called a *quasi-conformal mapping* if and only if f is the solution to the *Beltrami equation*:

$$\frac{\partial f}{\partial \bar{z}} = \mu(z) \frac{\partial f}{\partial z}$$

for some complex-valued function μ with $\|\mu(z)\|_\infty < 1$. If $\mu(z) = 0$, then the Beltrami equation becomes the Cauchy-Riemann equation, and the mapping is conformal. μ is called the *Beltrami coefficient* of f , and is usually denoted as μ_f .

$$K[f] = \frac{1 + \|\mu_f\|_\infty}{1 - \|\mu_f\|_\infty}$$

is called the *maximal dilation* of f .

In the local parameter domain around a point p , the diffeomorphism f can be approximated with respect to the local parameter by $f(z) = f(p) + f_z(p)z + f_{\bar{z}}(p)\bar{z} = f(p) + f_z(p)(z + \mu(p)\bar{z})$. It can be viewed as a translation to $f(p)$, together with a stretch map $S(z) = z + \mu(p)\bar{z}$ multiplied by $f_z(p)$. The translation and the scalar multiplication is conformal, so the conformality distortion of $f(z)$ is due to $S(z)$. The map $S(z)$ will stretch an infinitesimal circle to an infinitesimal ellipses, and the axis and magnitude of the maximal magnification and maximal shrinkage can be determined by $\mu(p)$. The angle of the maximal magnification direction is $\arg(\mu(p))/2$ with magnitude $1 + |\mu(p)|$, while the axis of maximal shrinkage is the orthogonal direction $(\arg(\mu(p)) - \pi)/2$ with magnitude $1 - |\mu(p)|$. Therefore, the Beltrami coefficient μ contains all the information about the map. See figure 1.1 for an illustration.

Theorem 1.3.1. (Riemann Mapping Theorem for Quasi-conformal Mapping) *Let D be a simply-connected domain in \mathbb{C} and $\mu(z) : D \rightarrow \mathbb{C}$ be a complex-valued function with $\|\mu(z)\|_\infty < 1$. Then there exists a quasi-conformal mapping $g : D \rightarrow \Delta$ whose Beltrami coefficient is equal to μ .*

The theorem states that there is a one-one correspondence between the space of quasi-conformal mappings and the space of Beltrami coefficient. We can reconstruct the quasi-conformal map from the associated Beltrami coefficient by solving the Beltrami equation.

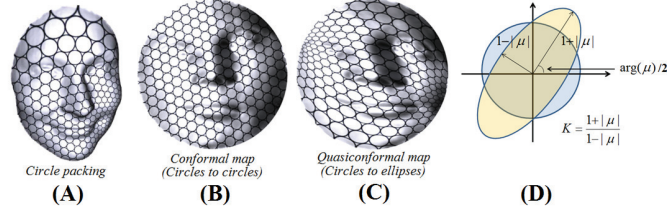


Figure 1.1: (A) shows a face mesh with the circle packing. (B) shows the conformal map from the face to a unit disk. The small circles on the face are mapped to small circles on the unit disk. (C) shows the quasi-conformal map. The small circles are mapped to small ellipses on the unit disk. (D) illustrates the effect of the Beltrami coefficient on the conformality distortion.

The Beltrami holomorphic flow is one of the method for computing the quasi-conformal maps from Beltrami coefficients.

Theorem 1.3.2. (Beltrami Holomorphic Flow) *There is a one-one correspondence between the set of all quasi-conformal mapping of the unit sphere $\mathbb{S}^2 = \bar{\mathbb{C}}$ that fix the points 0, 1 and ∞ and the set of all smooth complex-valued function μ on \mathbb{S}^2 such that $\|\mu\|_\infty < 1$. The solution f^μ of the Beltrami equation depends holomorphically on μ .*

Let $\{\mu(t)\}$ be a family of Beltrami coefficient with t as a parameter, and that μ can be written as

$$\mu(t)(z) = \mu(z) + t\nu(z) + t\varepsilon(t)(z)$$

for all $z \in \mathbb{C}$, where $\mu \in C^\infty(\mathbb{C})$ and $\nu, \varepsilon(t) \in L^\infty(\mathbb{C})$ with $\|\varepsilon(t)\|_\infty \rightarrow 0$ as $t \rightarrow 0$. Then for all $w \in \mathbb{C}$, we have

$$f^{\mu(t)}(w) = f^\mu(w) + tV(f^\mu, \nu)(w) + o(|t|)$$

on \mathbb{C} as $t \rightarrow 0$, where

$$V(f^\mu, \nu)(w) = -\frac{f^\mu(w)(f^\mu(w) - 1)}{\pi} \int_{\mathbb{C}} \frac{\nu(z)((f^\mu)_z(z))^2}{f^\mu(z)(f^\mu(z) - 1)(f^\mu(z) - f^\mu(w))} dx dy.$$

It gives us the variation of f^μ under the variation of μ explicitly.

Given the target μ , we can then flow the initial map f_0 , usually the identity map, iteratively to f^μ by

$$f_{k+1} = f_k + V\left(f_k, \frac{\mu}{N}\right), \quad k = 0, 1, \dots, N-1$$

where N is the number of iterations.

The fixed points can be arbitrarily chosen. Given a quasi-conformal map $f : \mathbb{S}^2 \rightarrow \mathbb{S}^2$, and three points $a, b, c \in \mathbb{S}^2$, we can find the unique Möbius transformations $\phi_1, \phi_2 : \mathbb{S}^2 \rightarrow \mathbb{S}^2$ such that $\phi_1(a) = 0$, $\phi_1(b) = 1$, $\phi_1(c) = \infty$ and $\phi_2(f(a)) = 0$, $\phi_2(f(b)) = 1$, $\phi_2(f(c)) = \infty$. Then the composition map $\tilde{f} = \phi_2 \circ f \circ \phi_1^{-1}$ is a quasi-conformal map fixing the points 0, 1 and ∞ . Thus, with the given Beltrami coefficient μ and a three points correspondence, we can reconstruct the quasi-conformal map by the Beltrami holomorphic flow.

The Beltrami holomorphic flow can be extended to the unit disk \mathbb{D} , where there is a one-one correspondence between the set of all quasi-conformal mappings with points 0 and 1 fixed and the set of Beltrami coefficient, with the variation of f^μ changed to

$$V(f^\mu, \nu)(w) = -\frac{f^\mu(w)(f^\mu(w) - 1)}{\pi} \left(\int_{\mathbb{D}} \frac{\nu(z)((f^\mu)_z(z))^2}{f^\mu(z)(f^\mu(z) - 1)(f^\mu(z) - f^\mu(w))} dx dy + \int_{\mathbb{D}} \frac{\overline{\nu(z)((f^\mu)_z(z))^2}}{f^\mu(z)(1 - \overline{f^\mu(z)}) (1 - \overline{f^\mu(z)}f^\mu(w))} dx dy \right).$$

For details about the Beltrami holomorphic flow, please refer to [20].

The reconstruction of the quasi-conformal maps from the Beltrami coefficient can also be done by the **Linear Beltrami Solver (LBS)**, which is developed in [15]. The basis idea is to discretize and approximate the Beltrami equation to a linear system, which is symmetric positive definite. The quasi-conformal map corresponding to the given Beltrami coefficient can be computed by solving the linear system. Landmark constrains can also be added to the linear system, and the linear Beltrami solver will

look for the best quasi-conformal mapping whose Beltrami coefficient is closest to the target one.

Definition 1.3.2. Under a boundary condition, a quasi-conformal map $f : D_1 \rightarrow D_2$ is called *extremal* if it satisfies

$$K[f] \leq K[g]$$

for all quasi-conformal map $g : D_1 \rightarrow D_2$ with the same boundary condition. It gives the least conformality distortion among all such mapping.

Definition 1.3.3. Let $f : D_1 \rightarrow D_2$ be a quasi-conformal map with Beltrami coefficient μ . f is said to be a *Teichmüller map* if there exist holomorphic function $\varphi : D_1 \rightarrow \mathbb{C}$ such that

$$\mu = k \frac{\bar{\varphi}}{|\varphi|}$$

for some constant $k < 1$. Therefore, the norm of the Beltrami coefficient of a Teichmüller map is constant, ie. $|\mu(v)| = k$ for all $v \in R_1$.

Teichmüller map is closely related to extremal map between simply connected surfaces. Under suitable boundary condition, an extremal map is a Teichmüller map. Therefore, by searching for a Teichmüller map with minimum norm, we can obtain an extremal map. [10, 6]

1.4 Laplace-Beltrami operator

Definition 1.4.1. Let f be a real-valued function defined on a Riemannian surface, the Laplace-Beltrami operator is defined by $\Delta f = \text{div}(\text{grad}(f))$. In the discrete case with triangular mesh T with vertices $V = \{p_i : i = 1, \dots, n\}$, functions are usually approximated by piece-wise linear functions. The function value of a point on a face is defined by linearly interpolating the value $f(p_i)$ for vertices p_i of the face. The discrete Laplace-Beltrami operator is expressed as

$$(\Delta f)(p_i) = \sum_{j \in N(i)} w_{ij} [f(p_j) - f(p_i)]$$

where $N(i)$ is the neighborhood of the vertex p_i , i.e. the vertices that are connected to vertex p_i by an edge, and w_{ij} is the weight defined on the edge $p_i p_j$. The edge weight is determined by the cotangent formula

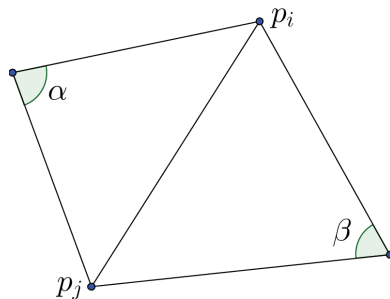


Figure 1.2:

$$w_{ij} = \begin{cases} \cot \alpha & \text{if } p_i p_j \text{ is on the boundary} \\ \frac{\cot \alpha + \cot \beta}{2} & \text{otherwise} \end{cases}$$

where α (and β) is the angle(s) against the edge $p_i p_j$, see figure 1.2.

The eigenfunctions of the discrete Laplace-Beltrami operator have some good properties regarding the global shape of the surface. We will rearrange the eigenfunctions according to the ascending order of the absolute value of the corresponding eigenvalues. The eigenfunction with the smallest eigenvalue is a constant function with eigenvalue zero and contains no information. The first non-trivial eigenfunction with smallest eigenvalue, also called the Fiedler vector, describes the longitudinal extension of the shape. For a snake-like structure, the Fiedler vector will attain its minimum value at one tip. The function will then increase following the shape and attain its maximum value at the other tip. The second and third non-trivial eigenfunctions share similar properties as the Fiedler vector, as they also increase from one end to another, but along the other two dimensions. Figure 1.3, showing the first three non-trivial eigenfunctions of a brainstem surface, illustrates this property.

When the surfaces are of similar shape and structure, such as the surfaces of a human organ of different people, the corresponding eigenfunctions will behave similarly.

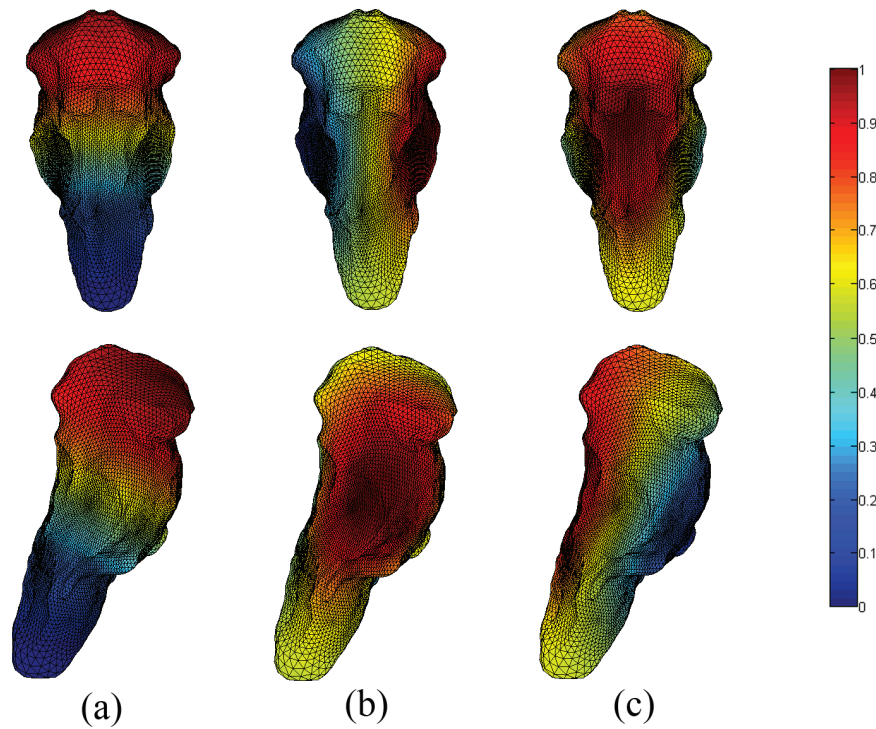


Figure 1.3: (a), (b) and (c) show the first three non-trivial eigenfunctions of a brainstem surface respectively. The first eigenfunction increases from bottom to top as shown in (a). The second eigenfunction increases from left to right as shown in (b). The third eigenfunction increases from back to front as shown in (c).

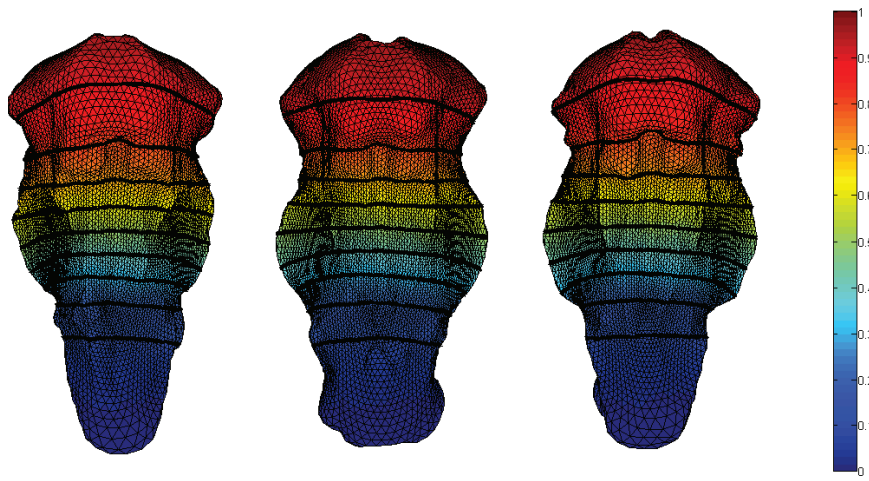


Figure 1.4: The first eigenfunction and the corresponding eigenloops of three different brainstem are plotted on the surfaces.

Figure 1.4 shows the first eigenfunction of three different brainstem surfaces, with the function value normalized to $[0, 1]$. Nine eigenloops, which are loops joined by points with the same function value, are drawn on each brainstem surface in figure 1.4. The eigenloops are chosen to be with function values $0.1, 0.2, \dots, 0.9$. We can see that the corresponding eigenloops of different brainstem surface are located at the same region of the brainstem. The eigenloops of the second and third eigenfunction are shown in figure 1.5 and 1.6 respectively, and the same properties can be observed.

With the above mentioned properties, we propose to use the first three non-trivial eigenfunction of the Laplace-Beltrami operator as a reference to different regions of the brainstem surface.

Definition 1.4.2. The discrete Laplace-Beltrami operator can be expressed in matrix form $\Delta f = L \times f(V)$, where $f(V)$ is a column vector with the value $f(p_i)$ in the i -th entry, and the matrix L is given by

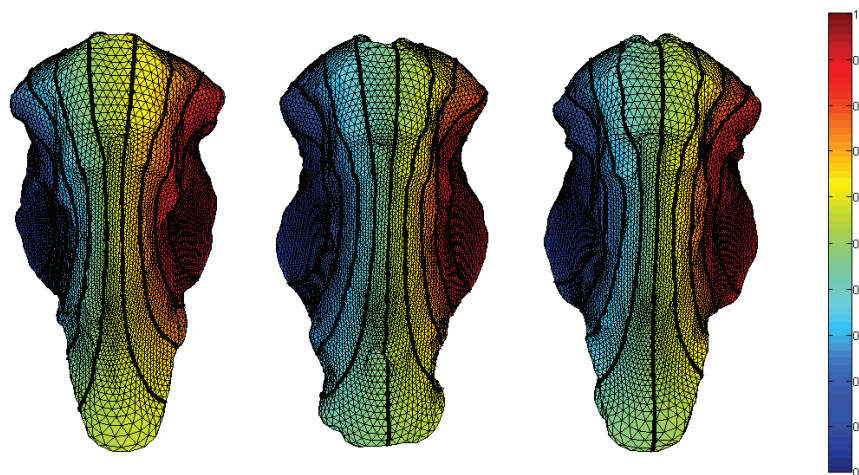


Figure 1.5: The second eigenfunction and the corresponding eigenloops of three different brainstem are plotted on the surfaces.

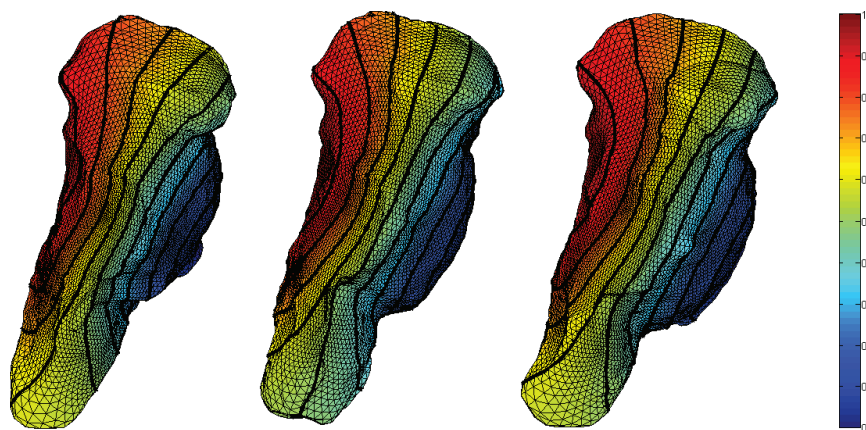


Figure 1.6: The third eigenfunction and the corresponding eigenloops of three different brainstem are plotted on the surfaces.

$$L_{ij} = \begin{cases} w_{ij} & \text{if } p_i p_j \text{ is an edge} \\ - \sum_{k \in N(i)} w_{ik} & \text{if } i = j \\ 0 & \text{otherwise} \end{cases}$$

The problem of finding eigenfunctions of Laplace-Beltrami operator is equivalent to finding eigenvectors of the matrix L . In this paper, we solve the eigenvectors by the built-in function of MATLAB. [24]

Chapter 2

Quasi-conformal Mapping For Medical Surface Registration

2.1 Introduction

In morphometry, when comparing two surfaces, we always want to find a one-one correspondence between the surfaces. There are two different types of registration: landmark-based and non-landmark-based. We will focus on landmark-based registration in this paper. A good landmark-based registration should be smooth and match the landmark points exactly, while the conformality distortion of the maps should be small. We proposed to apply the Quasi-conformal (QC) iteration developed in [15] to compute the Teichmüller extremal maps (T-map) on medical surfaces.

2.2 Quasi-conformal (QC) iteration

Recall that there is a one-one correspondence between quasi-conformal maps and Beltrami coefficient, and with the Linear Beltrami Solver (LBS) developed in [15], we can reconstruct the diffeomorphism from the associate Beltrami coefficient effectively by

solving a linear system. The space of Beltrami coefficient is easier to be manipulated than the space of quasi-conformal mappings. Therefore, Lui et. al. [15] proposed to find the Teichmüller map by finding the optimal Beltrami coefficient that minimize an energy functional measuring the conformality distortion. The Teichmüller extremal map is then reconstructed from the optimal Beltrami coefficient by LBS.

2.2.1 Computing Beltrami coefficient

Given the triangular mesh (V, F) of a domain $D \subset \mathbb{C}$, and the diffeomorphism $f = (f_1, f_2) : D \rightarrow \mathbb{C}$, we would like to compute the Beltrami coefficient of f on each face of D . The Beltrami equation $\frac{\partial f}{\partial \bar{z}} = \mu_f \frac{\partial f}{\partial z}$ can be explicitly written as

$$\mu_f = \left(\left(\frac{\partial f_1}{\partial x} - \frac{\partial f_2}{\partial y} \right) + i \left(\frac{\partial f_2}{\partial x} + \frac{\partial f_1}{\partial y} \right) \right) / \left(\left(\frac{\partial f_1}{\partial x} + \frac{\partial f_2}{\partial y} \right) + i \left(\frac{\partial f_2}{\partial x} - \frac{\partial f_1}{\partial y} \right) \right),$$

where the partial derivatives $\frac{\partial f_i}{\partial x}$ and $\frac{\partial f_i}{\partial y}$ on a face T can be found by solving the gradient $\nabla_T f_i = \left(\frac{\partial f_i}{\partial x}, \frac{\partial f_i}{\partial y} \right)^T$:

$$\begin{pmatrix} v_1 - v_0 \\ v_2 - v_0 \end{pmatrix} \nabla_T f_i = \begin{pmatrix} \frac{f_i(v_1) - f_i(v_0)}{|v_1 - v_0|} \\ \frac{f_i(v_2) - f_i(v_0)}{|v_2 - v_0|} \end{pmatrix},$$

where v_0, v_1 and v_2 are the three vertices of T . Then the Beltrami coefficient on each face can be found.

2.2.2 Main algorithm

Given the triangular mesh (V, F) of a domain $D_1 \subset \mathbb{C}$, a domain $D_2 \subset \mathbb{C}$ of the same topology, and the boundary condition $g : \partial D_1 \rightarrow \partial D_2$, we would like to compute

the Teichmüller extremal mapping $f : D_1 \rightarrow D_2$ such that $f|_{\partial D_1} = g$ with minimum conformality distortion.

Finding a Teichmüller map is equivalent to finding a function $f : D_1 \rightarrow D_2$ that satisfies

$$\frac{\partial f}{\partial \bar{z}} = k \frac{\bar{\varphi}}{|\varphi|} \frac{\partial f}{\partial z}, \quad f|_{\partial D_1} = g$$

for some constant k and holomorphic function $\varphi : D_1 \rightarrow \mathbb{C}$. A Teichmüller map f is called extremal if the infinite norm of the Beltrami coefficient associated is minimum among all Teichmüller maps with the same boundary constrain, i.e. for all $h : D_1 \rightarrow D_2$, satisfying $h|_{\partial D_1} = g$, we have

$$\|\mu(f)\|_\infty \leq \|\mu(h)\|_\infty.$$

The Teichmüller extremal mapping can be formulated as the following optimization problem:

$$\min_f \|\mu(f)\|_\infty + \|\nabla |\mu(f)|\|_2^2$$

subject to $f|_{\partial D_1} = g$. The first term of the energy functional is measuring the maximal conformality distortion, while the second term measures the smoothness of $|\mu(f)|$. For a Teichmüller extremal map, the first term of the energy functional is minimized, while the second term will be zero, as the norm of the Beltrami coefficient is constant. Therefore, the minimizer of the energy functional is the Teichmüller extremal map.

Since there is a one-one correspondence between the set of quasi-conformal mappings and the set of Beltrami coefficient, the optimization problem is equivalent to

$$\min_{\nu} \|\nu\|_{\infty} + \|\nabla |\nu|\|_2^2$$

subject to $\nu = \mu(f)$, $\|\nu\|_{\infty} < 1$, and $f|_{\partial D_1} = g$.

The advantage of minimizing the energy functional with respect to the Beltrami coefficient instead of the mapping is that the diffeomorphic property can be controlled easier. The mapping is guaranteed to be diffeomorphic if the norm of the Beltrami coefficient is less than 1. Therefore, by enforcing that $\|\nu\|_{\infty} < 1$, the map f^{ν} must be a diffeomorphism.

In order to find the Teichmüller extremal map, the Beltrami coefficient is iteratively modified through an iterative scheme called the Quasi-conformal (QC) iteration.

An initial map f_0 is constructed by the Linear Beltrami Solver (LBS) with the boundary constrain g and the target Beltrami coefficient $\mu_0 = 0$. As boundary constrains are enforced, the mapping found may not be conformal, i.e. $\mu(f_0) \neq 0$. LBS simply find the best quasi-conformal map whose Beltrami coefficient is closest to the desire one. Secondly, the Beltrami coefficient of f_0 is computed and denoted as ν_0 . Thridly, we apply the Laplace smoothing \mathfrak{L} , defined by

$$\mathfrak{L}(\nu(v)) = \frac{\sum_{u \in N(v)} \nu(u)}{\sum_{u \in N(v)} 1}$$

where $N(v)$ is the neighborhood of face v , on ν_0 to get $\tilde{\mu}_1$, which replaces the value of each face by the average value of the neighboring faces. Then, we apply an averaging \mathcal{A} , defined by

$$\mathcal{A}(\mu(v)) = \frac{\mu(v) \sum_{u \in F} |\mu(u)|}{|\mu(v)| \sum_{u \in F} 1}$$

on $\tilde{\mu}_0$ to obtain μ_1 , where the norm of the complex-valued μ_1 is re-scaled to the average of the norm of $\tilde{\mu}_0$. The Laplace smoothing aims at lowering the norm of the Beltrami coefficient, which correspond to the first term of the energy functional, while the averaging aims at minimizing the second term of the energy functional, ensuring the Beltrami coefficient to be of Teichmüller type. The next mapping f_1 is then computed by LBS with the boundary constrain and the target Beltrami coefficient set to be μ_1 . These steps are repeated until the Beltrami coefficient converges. The resultant f_n will be the Teichmüller map, and its Beltrami coefficient ν_n will be the smallest among all quasi-conformal maps satisfying the boundary conditions. The algorithm is summarized in algorithm 1.

Algorithm 1 Quasi-conformal iteration

Input: Triangular meshes (V, F) and the boundary constrains g

Output: Teichmüller extremal map f and the corresponding Beltrami coefficient ν

- 1: Compute the initial mapping $f_0 = \mathbf{LBS}(\mu_0 := 0, g)$
 - 2: Set $\nu_0 = \mu(f_0)$
 - 3: **while** $||\nu_n - \nu_{n-1}|| \geq \epsilon$ **do**
 - 4: Set $\mu_{n+1} = \mathcal{A}(\mathfrak{L}(\nu_n))$
 - 5: Set $f_{n+1} = \mathbf{LBS}(\mu_{n+1}, g)$
 - 6: Set $\nu_{n+1} = \mu(f_{n+1})$
 - 7: **end while**
 - 8: **return** f_n, ν_n
-

Additional landmark constrains can be added to the algorithm as the Linear Beltrami Solver can tackle with lots of landmarks even with large deformation. See [15] for more details about the Linear Beltrami Solver and the QC iteration.

2.3 Experimental result and conclusion

In this paper we applied the QC iteration to find the Teichmüller extremal map (T-map) between brainstem surfaces and teeth surfaces taken from MRI. Landmarks are manually taken from the surfaces.

2.3.1 Brainstem

The brainstem is a part of the human brain. It is a key organ in the body balance control system and plays an important role in the regulation of cardiac and respiratory function. It may also contribute to the Adolescent Idiopathic Scoliosis (AIS). Therefore, we would like to find a one-one corresponding registration between brainstem surfaces in order to detect the local shape difference.

Landmark points are drawn on three brainstem surfaces manually, as shown in figure 2.1, 2.2 and 2.3 respectively.

As the bottom part of a brainstem surface contains not much information, it is removed from the surface. The open surface is then mapped to the unit disk by conformal mapping. This process is shown in figure 2.4. The mean curvature of the brainstem surface is calculated. It is then plotted on the surfaces and disk as texture, with color red representing positive mean curvature and blue representing negative mean curvature. The red dots are the landmark points.

With the brainstem surfaces and corresponding landmark points mapped to unit disk, we applied the QC iteration to find the Teichmüller maps from brainstem surface A to B, and from A to C.

For simplicity, we further pick 4 landmark points on the boundary of each unit

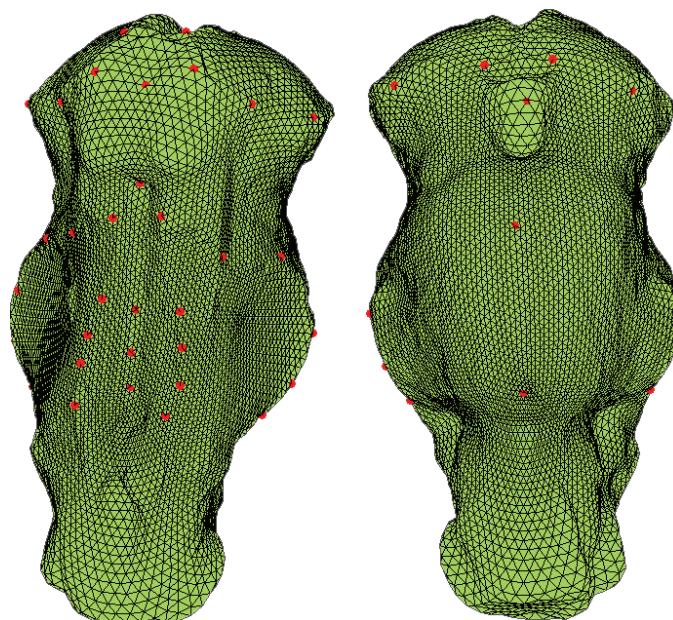


Figure 2.1: The landmark points are plotted on brainstem surface A as red dots.

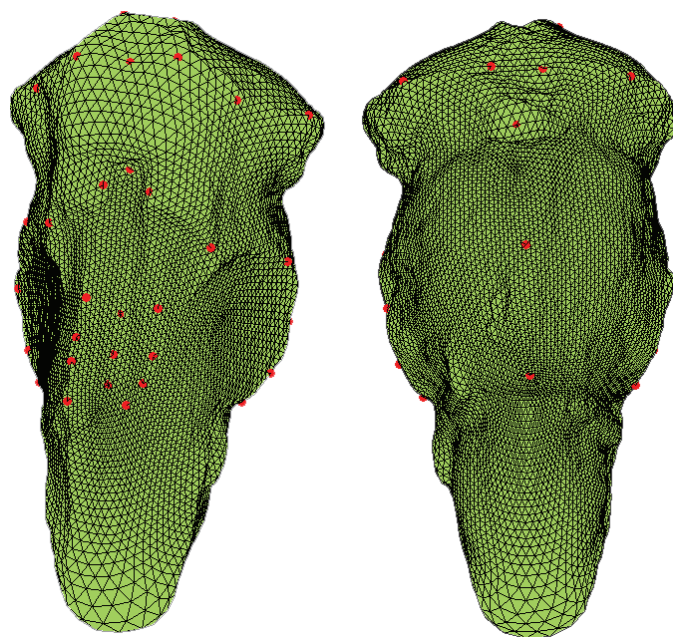


Figure 2.2: The landmark points are plotted on brainstem surface B as red dots.

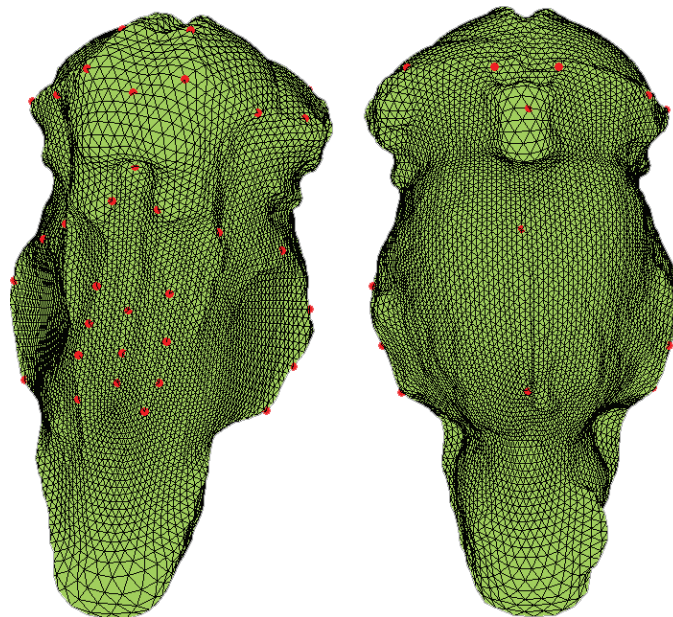


Figure 2.3: The landmark points are plotted on brainstem surface C as red dots.

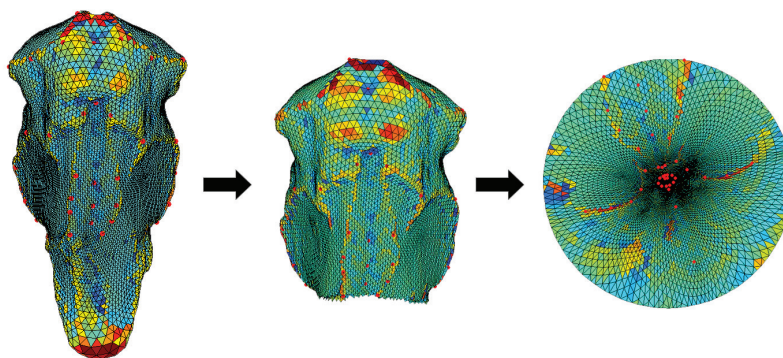


Figure 2.4: The bottom part of the brainstem surface B is removed and then mapped to the unit disk. The mean curvature is plotted to better visualize the mapping.

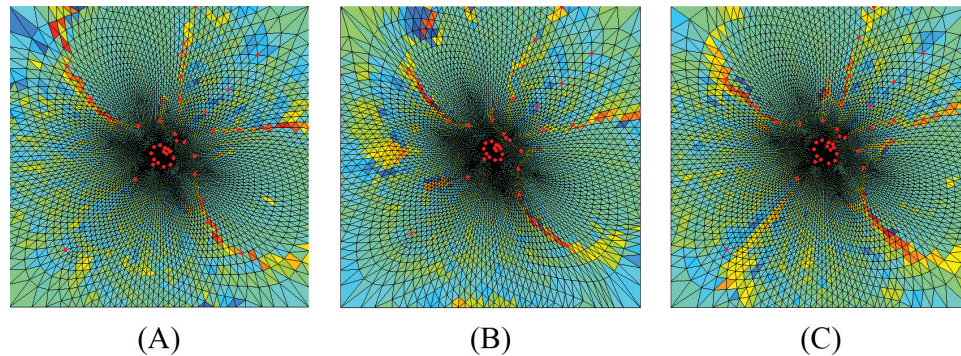


Figure 2.5: The three brainstem surfaces A, B and C are mapped to squares. The mean curvature and landmark points are plotted on each square as texture and red dots respectively.

disk and map them to a square with the 4 landmark points as corners. Figure 2.5 shows the brainstem surfaces mapped to squares, with mean curvature as texture and landmark points plotted on the squares

Figure 2.6 shows the Teichmüller extremal map from A to B found by the QC iteration. (a) shows the mesh grid and landmark points of A mapped by the T-map, while (b) shows the original mesh grid and landmark points of B. It can be shown that the landmark points of A are mapped exactly to the landmark points of B. The histogram in (c) shows that the norm of the Beltrami coefficient is concentrated in one value, and all values are less than 1, which indicate that it is a Teichmüller map and there is no overlapping in the mapping.

Figure 2.7 shows the diffeomorphism found by the QC iteration from brainstem surface A to C. The histogram shows that the norm of the Beltrami coefficient is concentrated in one value, which indicate that it is a Teichmüller map. There is no overlapping.

By linear interpretation, we can reconstruct the brainstem surfaces from the square

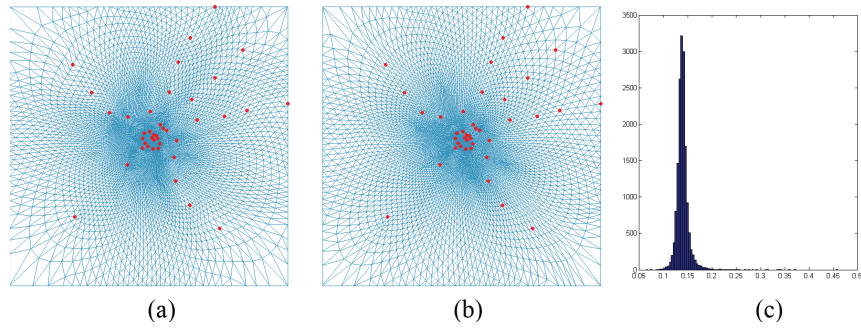


Figure 2.6: Teichmüller extremal map from brainstem A to B. (a) shows the mesh grid and landmark points of A mapped by the T-map. (b) shows the original mesh grid and landmark points of B. (c) shows the histogram of the norm of the Beltrami coefficient of the map.

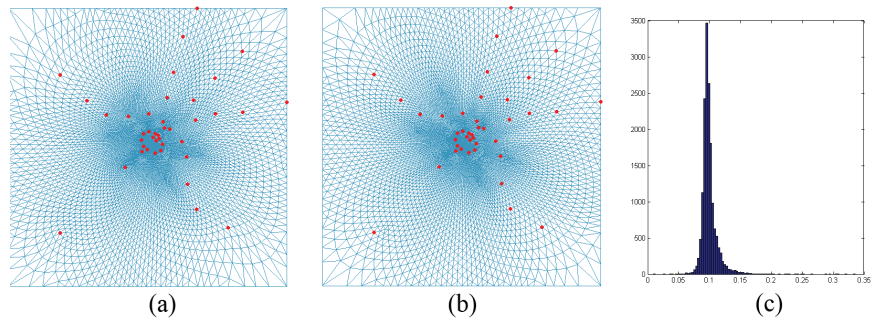


Figure 2.7: Teichmüller extremal map from brainstem A to C. (a) shows the mesh grid and landmark points of A mapped by the T-map. (b) shows the original mesh grid and landmark points of C. (c) shows the histogram of the norm of the Beltrami coefficient of the map.

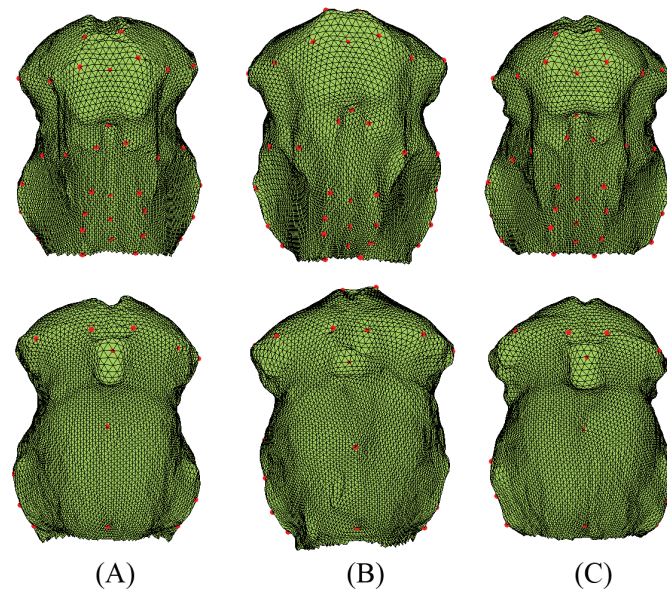


Figure 2.8: (A) shows the original brainstem surface A. (B) and (C) show the reconstructed brainstem surface from the Teichmüller maps from A, by the QC iteration. The red dots are the landmark points.

mesh. The resultant meshes will have the same number of vertices and the same connection between vertices. The one-one correspondence between the brainstem surfaces can then be achieved. Figure 2.8 show the reconstructed brainstem surfaces B and C, along with the original brainstem surface A. It can be observed that the structure of the triangular mesh are the same.

2.3.2 Teeth

Tooth A and tooth B are two molars of the same position taken from two different people. The triangular meshes are taken from the crown of the two teeth. Landmark points, such as the cusps, ridges and valleys, are manually located on the teeth surfaces. 4 points are taken from the boundary of the teeth surfaces, and the teeth surfaces are then mapped conformally to a square, with those 4 points as the corners.

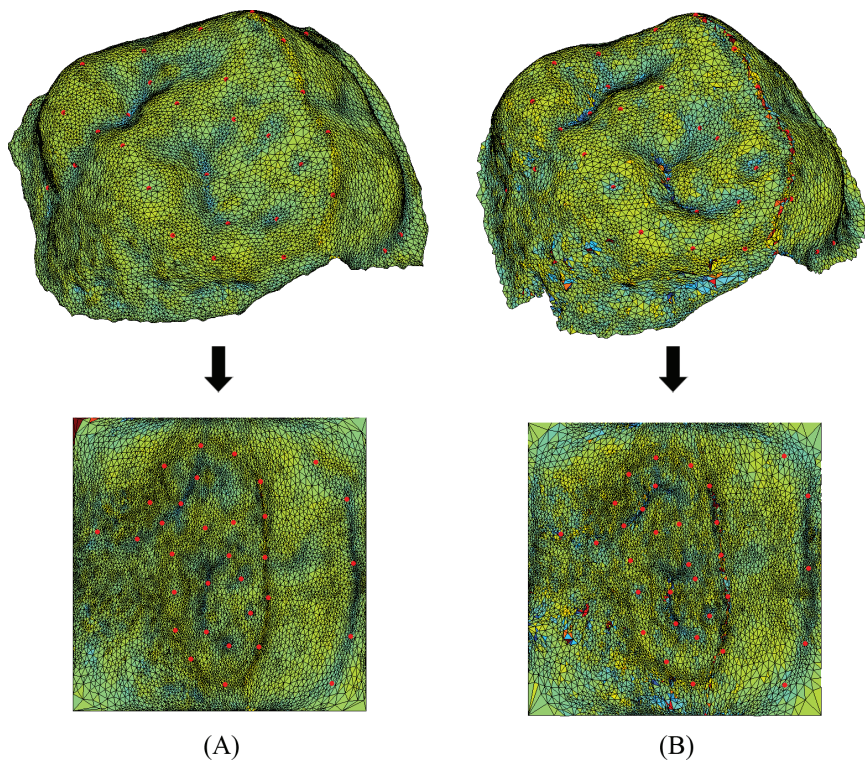


Figure 2.9: The upper images are the teeth surfaces taken from tooth A and B. The lower images are the square meshes mapped conformally from the teeth surfaces. Landmark points are plotted on the surfaces as red dots. Mean curvature of the teeth surfaces are plotted on the meshes as texture.

Figure 2.9 shows the teeth surfaces A and B, and the square meshes mapped by conformal maps. Landmarks points are plotted on the meshes as red dots, and the mean curvature of the teeth surfaces are plotted on the meshes as texture, with color red indicating region of positive curvature and blue indicating region of negative curvature.

Figure 2.10 shows the Teichmüller extremal map from tooth A to tooth B found by the QC iteration. (a) shows the mesh grid and landmark points of A mapped by the T-map, while (b) shows the original mesh grid and landmark points of B. It can be shown that the landmark points of A are mapped exactly to the landmark

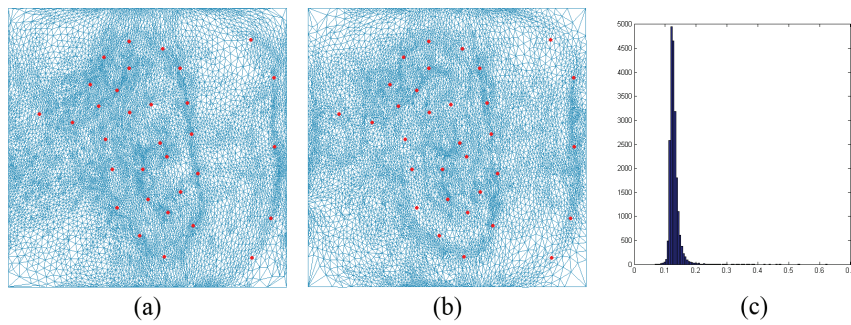


Figure 2.10: Teichmüller extremal map from tooth A to B. (a) shows the mesh grid and landmark points of A mapped by the T-map. (b) shows the original mesh grid and landmark points of B. (c) shows the histogram of the norm of the Beltrami coefficient of the map.

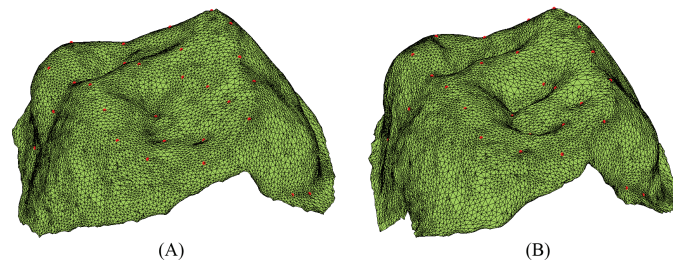


Figure 2.11: (A) shows the original tooth A. (B) shows the reconstructed tooth surface B from the Teichmüller extremal map obtained by the QC iteration. The red dots are the landmark points.

points of B. The histogram in (c) shows that the norm of the Beltrami coefficient is concentrated in one value, and all values are less than 1, which indicate that it is a Teichmüller map and there is no overlapping in the mapping.

By linear interpretation, we can reconstruct the teeth surfaces from the square mesh. The resultant meshes will have the same number of vertices and the same connection between vertices. The one-one correspondence between the teeth surfaces can then be achieved. Figure 2.11 shows the reconstructed tooth surface B and the original tooth A. It can be observed that the structure of the triangular mesh are the same.

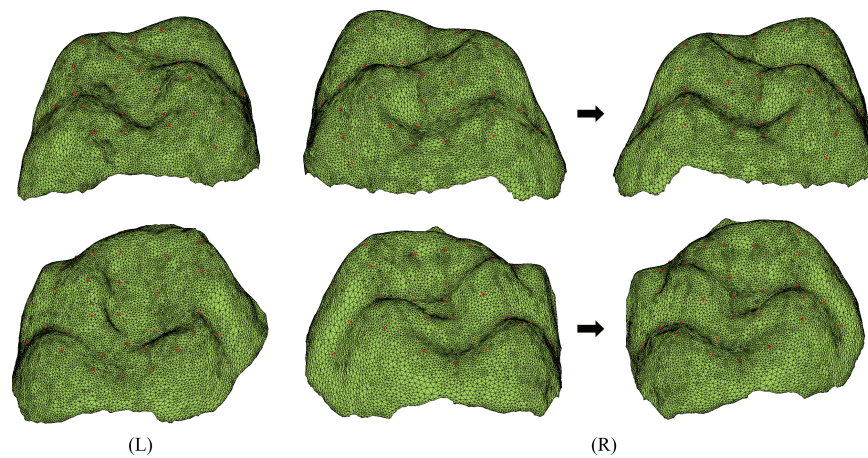


Figure 2.12: (L) shows the landmark points plotted on tooth L as red dots. (R) shows the landmark points plotted on tooth R and the flipped tooth R as red dots.

Tooth L and tooth R are two molar of the same position but on different side of the same person. The tooth L is taken from the left side, while the tooth R is taken from the right side. The images in the left and middle in Figure 2.12 shows the triangular meshes of the two teeth respectively, with landmark points plotted on the surfaces as red dots. The two meshes are of opposite orientation, so the mesh of tooth R is flipped, by taking negative on the x -coordinate of the vertices and flipping the faces. The flipped tooth R is shown in the images in the right in Figure 2.12. 4 points are taken from the boundary of the teeth surfaces, and the surfaces are then mapped conformally to squares with those 4 points as corners. Figure 2.13 shows the mapping from the teeth surfaces to squares. The mean curvature of the teeth surfaces are plotted on the meshes as texture.

Figure 2.14 shows the Teichmüller extremal map from tooth L to tooth R found by the QC iteration. The landmark points are exactly matched.

By linear interpretation, we can reconstruct the teeth surfaces from the square mesh. The resultant meshes will have the same number of vertices and the same

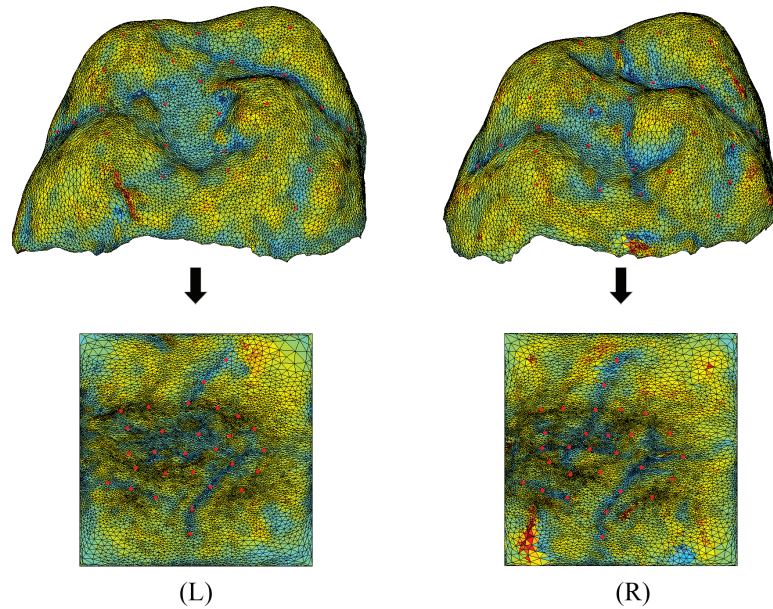


Figure 2.13: The upper images are the teeth surfaces taken from tooth L and R. The lower images are the square meshes mapped conformally from the teeth surfaces. Landmark points are plotted on the surfaces as red dots. Mean curvature of the teeth surfaces are plotted on the meshes as texture.

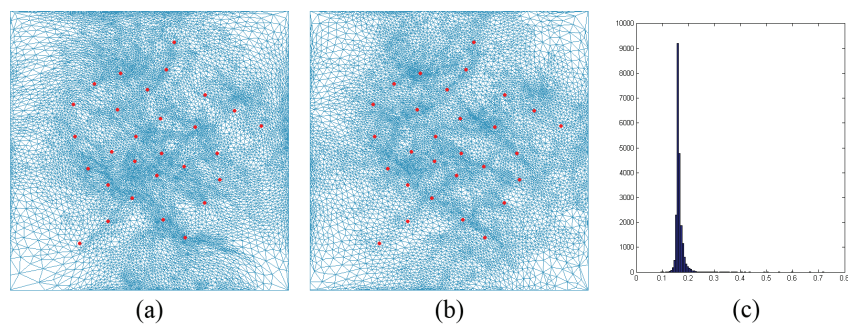


Figure 2.14: Teichmüller extremal map from tooth L to tooth R. (a) shows the mesh grid and landmark points of L mapped by the T-map. (b) shows the original mesh grid and landmark points of R. (c) shows the histogram of the norm of the Beltrami coefficient of the map.

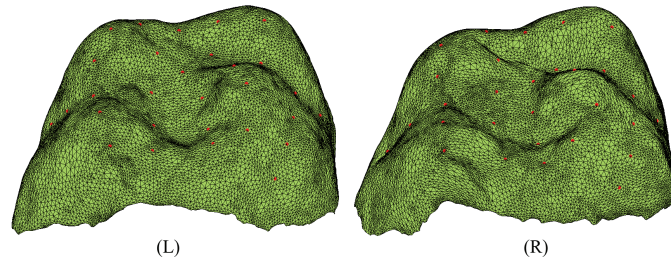


Figure 2.15: (L) shows the original tooth L. (R) shows the reconstructed tooth surface R from the Teichmüller extremal map obtained by the QC iteration. The red dots are the landmark points.

connection between vertices. The one-one correspondence between the teeth surfaces can then be achieved. Figure 2.15 shows the reconstructed tooth surface B and the original tooth A. It can be observed that the structure of the triangular mesh are the same.

2.3.3 Conclusion

Experimental results show that the QC iteration developed in [15] is effective in finding landmark-matching registrations for shape morphometry of medical images.

The Teichmüller extremal maps (T-maps) between surfaces are found effectively. The landmarks are exactly matched by the T-map and there are no overlaps in the maps. The surfaces can be reconstructed with meshes having the same number of vertices and the same connection between vertices. The one-one correspondence between the surfaces can then be achieved. The diffeomorphism is extremal and the conformality distortion is minimized among all diffeomorphism with the same landmark constrains. Table 2.1 shows the computation time for finding the Teichmüller extremal maps along with the number of vertices and landmarks for the four pairs of surfaces.

	Time (s)	# of vertices	# of landmarks
Brainstem A and B	2.903	8132	40
Brainstem A and C	2.228	8132	40
Tooth A and B	3.316	10572	32
Tooth L and R	3.313	11087	29

Table 2.1: The computation time for finding the Teichmüller extremal maps along with the number of vertices and landmarks for the four pairs of surfaces.

Chapter 3

Feature Extraction of Anatomic Structure

3.1 Introduction

There are three kinds of method to extraction landmarks on a surface: manually, automatically, and semi-automatically. Manual landmark extraction is the most accurate, as it can utilize the most of the knowledge of medical experts to locate the landmark exactly. However, it is very time-consuming. It is good for small-scale experiment, but not suitable for a large-scale one. An automatic landmark extraction method usually utilize the local geometric structures, such as the gaussian, mean and principal curvature and the principal directions, to locate ridges, valleys and other features on the surface. Those vertices and edges are then filtered, joined and smoothed to form feature curves. Automatic landmark extraction is fast, but we have not much control on the landmarks extracted. For most automatic landmark extraction algorithm, the “best” feature curves will be selected based on some criteria, but there is no guarantee that the “best” ones are consistent features instead of abnormalities, whereas some of the desire features may not be in the best five or ten. Labeling the features will

be another problem for an automatic landmark extraction algorithm. Some curves can be extracted, but it is usually difficult to ask a computer to distinguish which curve is the specific landmark. Therefore, we propose a semi-automatic landmark extraction algorithm, which requires background knowledge on the specific surface to assign different parameters for each landmark. For each landmark, some times are needed to spend on assigning the parameters, but the computation will be automatic and it can deal with any number of samples.

There are some consistent landmarks with high mean curvature on a brainstem surface. We will develop an algorithm using the eigenfunction of Laplace-Beltrami operator and Chan-Vese segmentation to extract the landmarks semi-automatically. The eigenfunction of Laplace-Beltrami operator are consistent on surfaces with similar structure and can be used as a reference to obtain the search region for a specific landmark. The high curvature landmark can then be segmented from the search region by the Chan-Vese segmentation by using the curvature as intensity of an image.

3.2 Chan-Vese segmentation

The Chan-Vese segmentation is a widely-used segmentation method that segment an image based on the intensity of the image. It can separate higher-intensity objects from the lower-intensity background of an image.

The basic idea is to use a level-set function to represent a contour, with positive value in the region inside the contour, and negative value outside the contour. The zero level-set of the function is the contour, lying in the boundary between the two regions. We find the function ϕ by minimizing the following energy functional:

$$\begin{aligned}
F(c_1, c_2, \phi) = & \mu \int_{\Omega} |\nabla H(\phi)| dA + \nu \int_{\Omega} H(\phi) dA + \lambda_1 \int_{\Omega} |u - c_1|^2 H(\phi) dA \\
& + \lambda_2 \int_{\Omega} |u - c_2|^2 (1 - H(\phi)) dA
\end{aligned}$$

where u is the input image, and the Heaviside function $H : \mathbb{R} \rightarrow \{0, 1\}$ is defined as

$$H(x) = \begin{cases} 1 & \text{if } x \geq 0 \\ 0 & \text{if } x < 0. \end{cases}$$

The first and second term of the energy functional are the regularization terms, measuring the length of the contour, and the area inside the contour respectively. Since ϕ is positive in the region inside the contour and negative outside, the value $H(\phi)$ is 1 inside the contour and 0 outside. Therefore, the third term of the energy functional is measuring the intensity difference $|u - c_1|^2$ among the region inside the contour, and the last term is measuring the intensity difference $|u - c_2|^2$ outside the contour.

When the image is consist of a background with lower intensity of an average c_2 and an object with higher intensity of an average c_1 , then c_1 , c_2 and ϕ with positive value in the higher-intensity region, negative value in the lower-intensity region, and value zero on the boundary, will minimize the energy functional. Therefore, by minimizing the energy functional, we can find a level-set function to represent the contour and segment the image.

For details, please refer to [2].

3.3 Proposed algorithm

There are some consistent high-curvature landmark feature located at the same region on brainstem surfaces. The first three non-trivial Laplace-Beltrami eigenfunctions, as discussed in section 1.4, will be able to locate each feature curve.

Let S be a brainstem surface with F , E , V be the triangular mesh, where F is the set of faces, E is the set of edges, and $V = \{p_i : i = 1, 2, \dots, n\}$ is the set of vertices. Let L be the Laplace-Beltrami matrix defined by

$$L_{ij} = \begin{cases} w_{ij} & \text{if } p_i p_j \in E \\ - \sum_{k \in N(i)} w_{ik} & \text{if } i = j \\ 0 & \text{otherwise} \end{cases}$$

where w_{ij} is the edge weight defined above in (1.4). We calculate the first three non-trivial eigenvector, denoted \tilde{f}_1 , \tilde{f}_2 and \tilde{f}_3 respectively, of L . Then we normalize the eigenvectors to the interval $[0, 1]$, with the value 0 assigned to a specific end and 1 to the other, for each of the three directions, ie.

$$f_i = \frac{\tilde{f}_i - \min(\tilde{f}_i)}{\max(\tilde{f}_i) - \min(\tilde{f}_i)}$$

for $i = 1, 2, 3$.

Then, by referring to a few controls, we find the appropriate set of ranges for each landmark. For example, the red curve in figure 3.1 (a) lies in the region with the first eigenvector in the range $[0.25, 0.75]$, the second eigenvector in the range $[0, 0.5]$, and the third eigenvector in the range $[0.25, 0.75]$. Let $V' = \{v \in V : f_1(v) \in [0.25, 0.75], f_2(v) \in [0, 0.5], f_3(v) \in [0.25, 0.75]\}$ and F' be the set of faces with all three vertices

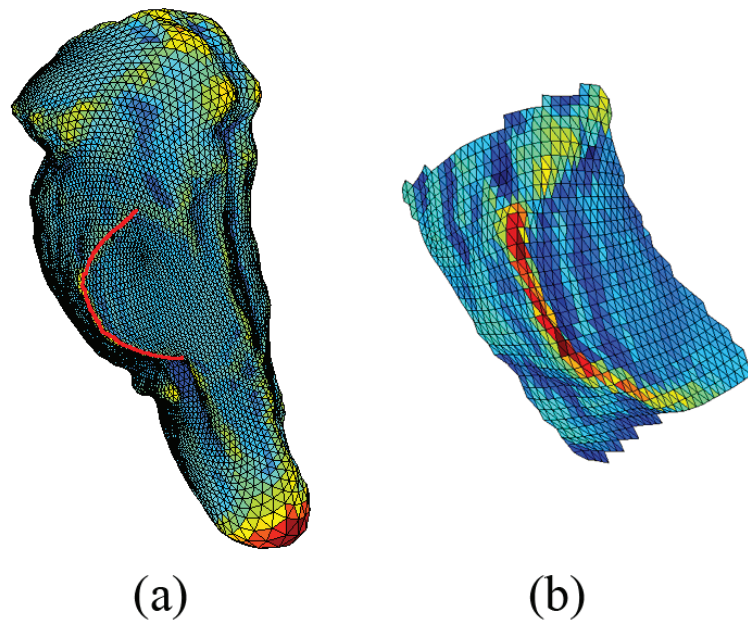


Figure 3.1: (a) shows the brainstem surface, with the red curve indicating a landmark feature curve. (b) is the separated new mesh, which contains the target feature curve. Mean curvature is plotted on the meshes as texture.

in V' . Then the vertices V' and faces F' in this search region is separated to form a new mesh, as shown in figure 3.1 (b).

By construction, the new mesh will be similar to a quadrilateral, and four corners can be easily located by eigenvectors, such as by finding the vertices that minimize $f_1 + f_3$, $f_1 - f_3$, $-f_1 - f_3$ and $-f_1 + f_3$ respectively for the example mentioned above. It is then mapped to a square with the four corners mapped to the corresponding corners and boundary vertex mapped to the corresponding edge. It can be done by the Linear Beltrami Solver with the above boundary condition and the target Beltrami coefficients set to zero. This is shown in figure 3.2.

The mean curvature of the vertices on the brainstem surface, denoted as $C_{\text{mean}} : V \rightarrow \mathbb{R}$, is then calculated. It is then smoothen by gaussian smoothing to get a wider

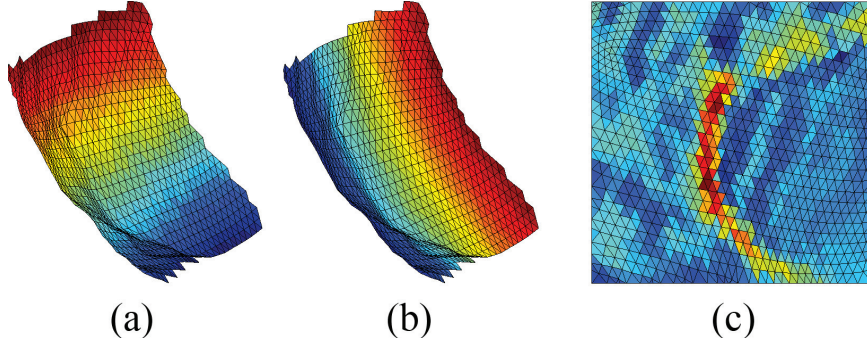


Figure 3.2: (a) and (b) show the first and third eigenvectors on the separated mesh. (c) shows the square mesh, with mean curvature of the brainstem surface as texture.

region of high-curvature points so that it can be segmented easier. It can be done by $C = G \times C_{\text{mean}}$, where C and C_{mean} are both arranged by the same order of V , and G is a matrix defined by

$$G_{ij} = \begin{cases} \frac{1}{\sqrt{2\pi\sigma^2}} e^{-|p_i - p_j|^2 / 2\sigma^2} & \text{if } p_i p_j \in E \\ \frac{1}{\sqrt{2\pi\sigma^2}} & \text{if } i = j \\ 0 & \text{otherwise} \end{cases}$$

where σ is the standard deviation.

Together with the mean curvature as intensity, the square mesh computed above can be treated as an image. By the Chan-Vese segmentation, we can segment the high-curvature region from the square. This region will be corresponding to the specific high-curvature landmark on the brainstem surfaces. Two end points are then located on the high-curvature region with the criteria that the mean curvature of the two end points should be high and they should be farthest apart. A curve is then drawn to join the two end points by finding the geodesic or the shortest path on the brainstem surface. The resultant curves will be the desired landmark curves.

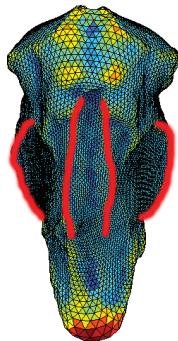


Figure 3.3: From left to right, the first, third, fourth and second landmarks are drawn manually on the brainstem surfaces as red curves.

3.4 Results and conclusion

17 brainstem surfaces taken from MRI is used to test the algorithm. There are four ridge that can be used as landmarks on each brainstem surface (see figure 3.3). The first and second ridges are two curves located on the edge of the ear-shape regions. The third and fourth are two straight ridges alongside the valley in the middle of the front side of the brainstem surface.

The first landmark is located in the set $V_1 = \{v \in V : f_1(v) \in [0.25, 0.75], f_2(v) \in [0, 0.5], f_3(v) \in [0.25, 0.75]\}$ and F_1 as the set of faces with all three vertices in V_1 . The surface $S_1 \subset S$ formed by V_1 and F_1 are of quadrilateral shape, and with f_1 increasing from one edge to the opposite, and f_3 increasing from the other direction. Figure 3.4 shows the surface S_1 with f_1, f_3 plotted on it. Then f_1 and f_3 are normalized to $[0, 1]$ again on V_1 , by

$$f'_1 = \frac{f_1 - \min_{V_1} f_1}{\max_{V_1} f_1 - \min_{V_1} f_1}$$

$$f'_3 = \frac{f_3 - \min_{V_1} f_3}{\max_{V_1} f_3 - \min_{V_1} f_3}$$

The vertices that minimize $f'_1 + f'_3, f'_1 - f'_3, -f'_1 - f'_3$ and $-f'_1 + f'_3$ respectively

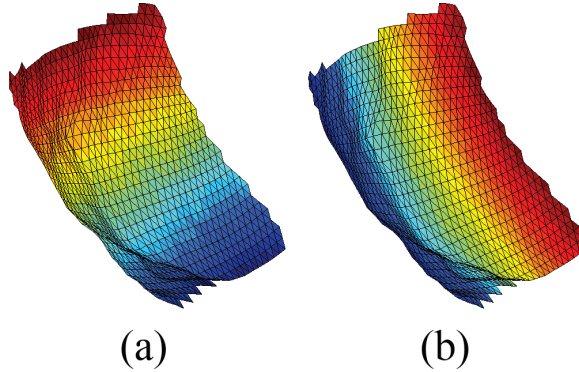


Figure 3.4: (a) and (b) show the surface S_1 with the first eigenvector f_1 and the third eigenvector f_3 plotted on it respectively.

are the 4 corners of the quadrilateral in counter-clockwise direction. By the Linear Beltrami Solver (LBS), we can find a quasi-conformal mapping $g : S_1 \rightarrow [0, 1] \times [0, 1]$ with the four corners mapped to the corresponding corners and boundary mapped to the corresponding boundary. With the mean curvature $C : V \rightarrow \mathbb{R}$ calculated and smoothed as in Section 3.3, we can find a piecewise linear intensity function $C_1 : [0, 1] \times [0, 1] \rightarrow \mathbb{R}$ with $C_1(g(v)) = C(v) \forall v \in V_1$ and the value of point inside a face be linearly interpolated by the value of the three vertices of the face. Using the intensity function C_1 , we get an image I with a background of lower-intensity and a crescentic object with higher-intensity (see figure 3.5). The latter corresponds to the high curvature landmark that we want to extract.

By Chan-Vese segmentation, the higher-intensity object \tilde{R}_1 can be segmented. By removing the smaller disconnected parts, we obtain a simply-connected region R_1 that contains the desire landmark. We map the region back to the brainstem surface S by g^{-1} (see figure 3.6). In figure 3.7, the normalized f_1, f_2, f_3 is plotted on the region. We find that the vertices that maximize $f_1 + f_3$ and $-f_1 + f_2 + f_3$ can be used as the starting and ending vertices of the landmark. By the Dijkstra's algorithm with

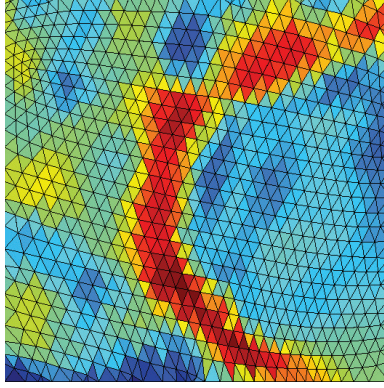


Figure 3.5: The square mesh S_1 with the intensity function C_1 . It consists of the red region of higher-intensity landmark and the greenish-blue background of lower-intensity.

edge weight of edge $p_i p_j$ being $w_{ij} = \frac{|p_i - p_j|}{C_{ij} + 1}$, where C_{ij} is the average mean curvature of p_i and p_j normalized to $[0, 1]$, we find a path in R_1 from the starting to the ending vertex that has a short distance while following the highest-curvature vertices. The resultant path is the desired landmark. Figure 3.8 shows the extracted landmark on three different brainstem surfaces.

The second landmark is in the opposite side of the first landmark, with regard to the second eigenvector, located in the set $V_2 = \{v \in V : f_1(v) \in [0.25, 0.75], f_2(v) \in [0.5, 1], f_3(v) \in [0.25, 0.75]\}$ and F_2 as the set of faces with all three vertices in V_2 . The surface $S_2 \subset S$ formed by V_2 and F_2 are of quadrilateral shape, and with f_1 increasing from one edge to the opposite, and f_3 increasing from the other direction. Figure 3.9 shows the surface S_2 with f_1, f_3 plotted on it.

Then f_1 and f_3 are normalized to $[0, 1]$ on V_2 by the similar way as on V_1 . The vertices that minimize $f'_1 + f'_3, -f'_1 + f'_3, -f'_1 - f'_3$ and $f'_1 - f'_3$ respectively are the 4 corners of the quadrilateral in counter-clockwise direction. The surface S_2 is mapped

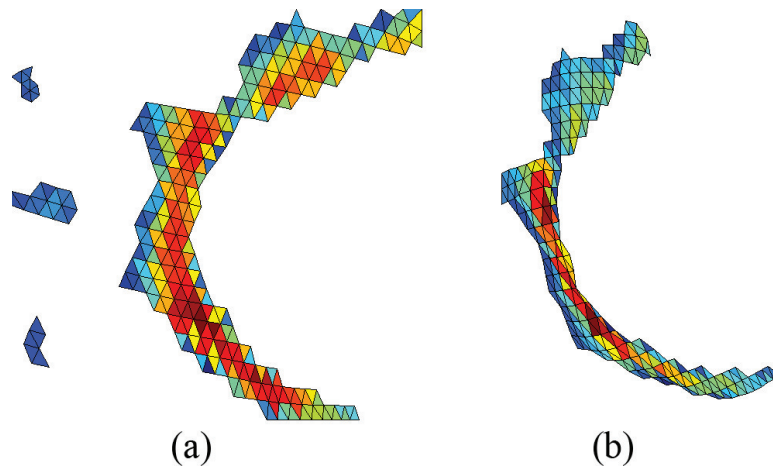


Figure 3.6: (a) shows the region segmented by the Chan-Vese segmentation. By removing the smaller disconnected parts and then mapped back to the brainstem surface, we obtained the region in (b).

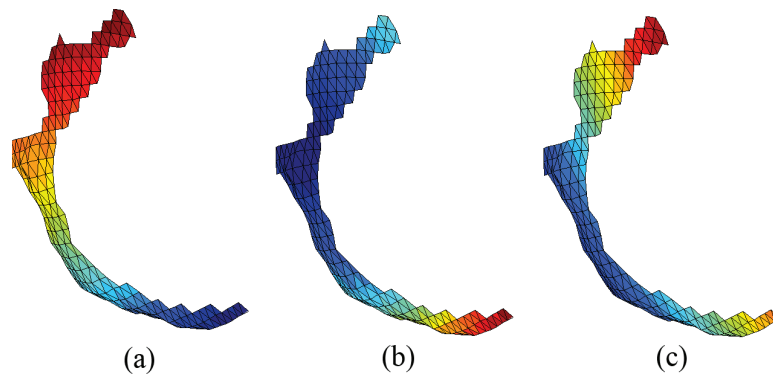


Figure 3.7: The first three eigenvectors f_1 , f_2 and f_3 are plotted on the segmented region in (a), (b) and (c) respectively.

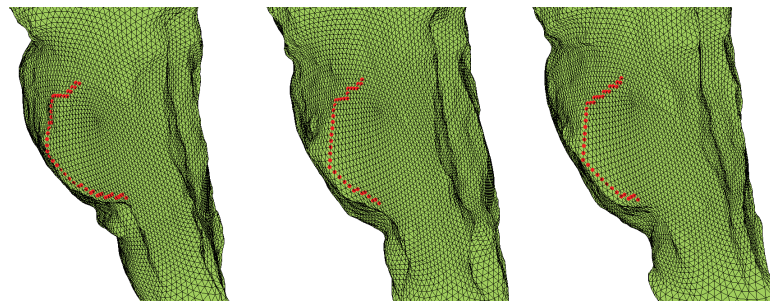


Figure 3.8: The first extracted landmarks of three different brainstem surfaces.

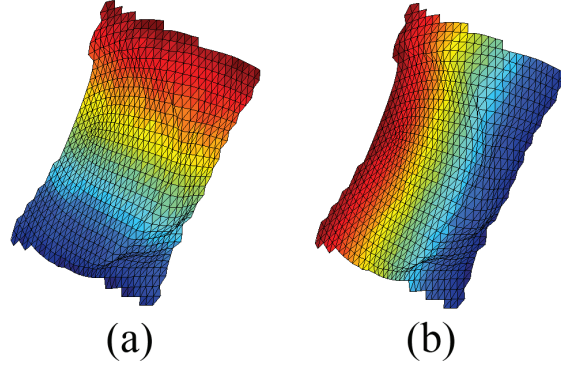


Figure 3.9: (a) and (b) show the surface S_2 with the first eigenvector f_1 and the third eigenvector f_3 plotted on it respectively.

to the square $[0, 1] \times [0, 1]$ by a quasi-conformal mapping found by LBS, and a piecewise linear intensity function C_2 can be found by similar way as C_1 . The figure 3.10 shows the image formed by the intensity function C_2 . We segment the higher-intensity region \tilde{R}_2 from the image by Chan-Vese segmentation, and obtained $R_2 \subset S$ that contains the desire landmark as shown in figure 3.11. Two end points defined as the vertices that maximize $f_1 + f_3$ and $-f_1 - f_2 + f_3$ respectively are joined by a path found by Dijkstra's algorithm. Figure 3.12 shows the extracted landmark on different brainstem surfaces.

By choosing the set $V_3 = \{v \in V : f_1(v) \in [0.22, 0.75], f_2(v) \in [0.25, 0.55], f_3(v) \in [0.5, 1]\}$ and $V_4 = \{v \in V : f_1(v) \in [0.22, 0.75], f_2(v) \in [0.45, 0.75], f_3(v) \in [0.5, 1]\}$, we can define surfaces $S_3, S_4 \subset S$ that contains the third and fourth landmark respectively. Figure 3.13 shows the surfaces S_3, S_4 cut from the brainstem S . By the above algorithm, we can extract the third and fourth landmarks, as shown in figure 3.14 and 3.15, respectively.

Figure 3.16 shows the four landmarks plotted on three brainstem surfaces. 17

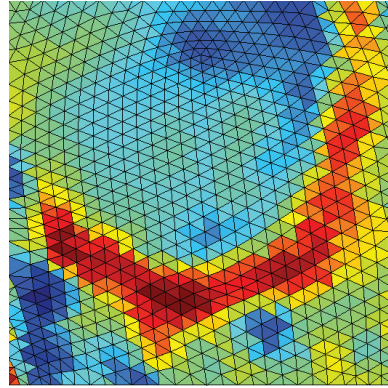


Figure 3.10: The square mesh S_1 with the intensity function C_1 . It consists of the red region of higher-intensity landmark and the greenish-blue background of lower-intensity.

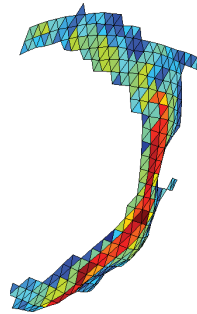


Figure 3.11: The region segmented by the Chan-Vese segmentation. The smaller disconnected parts are removed and it is mapped back to the brainstem surface.

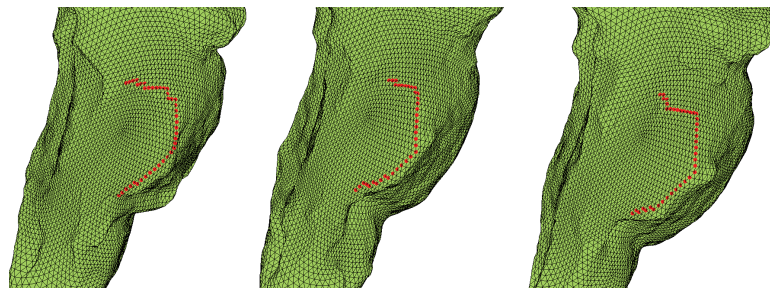


Figure 3.12: The second extracted landmarks of three different brainstem surfaces.

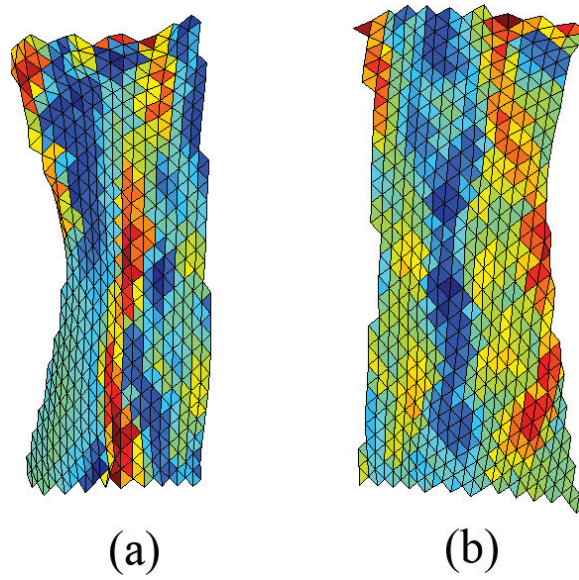


Figure 3.13: (a) and (b) show the surface S_3 and S_4 respectively.

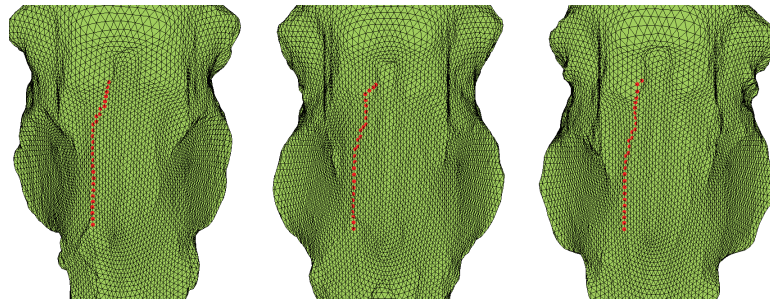


Figure 3.14: The third extracted landmarks of three different brainstem surfaces.

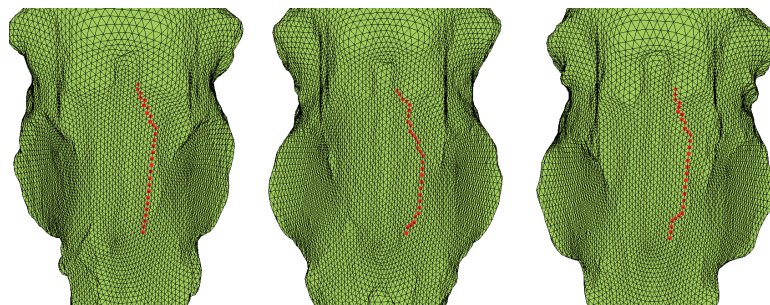


Figure 3.15: The fourth extracted landmarks of three different brainstem surfaces.

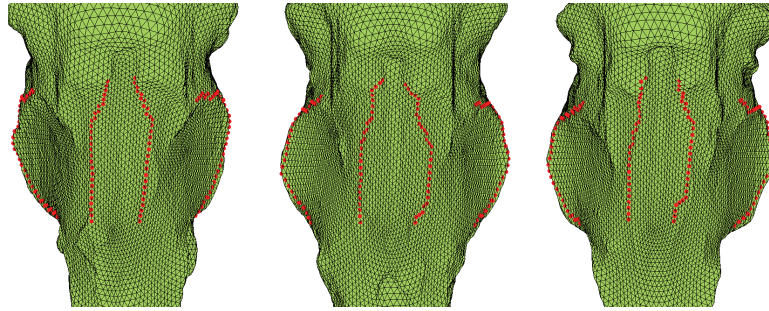


Figure 3.16: The four extracted landmarks of three different brainstem surfaces.

	1st landmark	2nd landmark	3rd landmark	4th landmark
Time(s)	2.45	3.23	2.30	2.14

Table 3.1: The average compute time to extract the 4 landmarks.

brainstem surfaces are tested with the algorithm. The resultant landmarks are consistent and lying on the ridges on the respective regions. It takes an average of 2.53 seconds to extract a landmark from a brainstem surface. Table 3.1 shows the average compute time to extract each of the 4 landmarks.

By customizing the search region and the search criteria for end points and landmark points, other feature landmarks can be extracted. The algorithm can also be applied to other surfaces.

Chapter 4

Conclusion

We proposed to apply the Quasi-conformal (QC) iteration proposed in [15] for landmark matching registration of medical images. The Teichmüller extremal maps (T-maps) between specimens are computed by the algorithm as the one-one corresponding registration. The idea of the QC iteration is to represent a quasi-conformal mapping by its associated Beltrami coefficient through the use of the Linear Beltrami Solver (LBS). The Beltrami coefficient is then optimized iteratively to minimize an energy functional measuring the conformality distortion and other factors. The resultant mappings are obtained from LBS with the optimal Beltrami coefficients. T-maps are advantageous as it minimizes the maximal conformality distortion. In this paper, real brainstem surfaces and Teeth surfaces taken from MRIs are used as the experiment subjects. Experimental results show that the algorithm is effective for computing the T-maps. Landmarks are exactly matched by the mappings. The computation time of the algorithm is short.

We also proposed a semi-automatic landmark extraction algorithm for brainstem surfaces, utilizing the geometric information on the surface. The first three non-trivial eigenvectors of the Laplace-Beltrami operator are used as a reference to indicate the

search region for a specific landmark feature curve. Then, by conformal mapping and the mean curvature of the surfaces, we created an image of the landmark in the search region. The Chan-Vese segmentation algorithm is applied on the image to segment the landmark, which can then be traced back to the brainstem surface. The experimental results show that the algorithm can extract the target landmark feature curves consistently and effectively.

Bibliography

- [1] F.L. Bookstein, *Morphometric tools for landmark data: geometry and biology*, Cambridge University Press, 1997.
- [2] T.F. Chan and L.A. Vese, *Active contours without edges*, Image Processing, IEEE Transactions on **10** (2001), no. 2, 266–277.
- [3] B. Chow and F. Luo, *Combinatorial ricci flows on surfaces*, Journal of Differential Geometry **63** (2003), no. 1, 97–129.
- [4] I.L. Dryden and K.V. Mardia, *Statistical shape analysis*, John Wiley and Sons, Chichester, England, 1998.
- [5] B. Fischl, M.I. Sereno, R.B.H. Tootell, A.M. Dale, et al., *High-resolution intersubject averaging and a coordinate system for the cortical surface*, Human brain mapping **8** (1999), no. 4, 272–284.
- [6] F.P. Gardiner and N. Lakic, *Quasiconformal teichmüller theory*, vol. 76, Amer Mathematical Society, 2000.
- [7] J. Glaunès, M. Vaillant, and M.I. Miller, *Landmark matching via large deformation diffeomorphisms on the sphere*, Journal of Mathematical Imaging and Vision **20** (2004), no. 1-2, 179–200.

- [8] X. Gu, Y. Wang, T.F. Chan, P.M. Thompson, and S.-T. Yau, *Genus zero surface conformal mapping and its application to brain surface mapping*, Medical Imaging, IEEE Transactions on **23** (2004), no. 8, 949–958.
- [9] X. Gu and S.-T. Yau, *Computing conformal structure of surfaces*, Communication in Information System **2** (2002), no. 2, 121–146.
- [10] ———, *Computational conformal geometry*, Intl Pr of Boston Inc, 2008.
- [11] M.K. Hurdal and K. Stephenson, *Discrete conformal methods for cortical brain flattening*, Neuroimage **45** (2009), no. 1, 86–98.
- [12] M. Jin, J. Kim, F. Luo, and X. Gu, *Discrete surface ricci flow*, Visualization and Computer Graphics, IEEE Transactions on **14** (2008), no. 5, 1030–1043.
- [13] A. Leow, C.L. Yu, S.J. Lee, S.C. Huang, H. Protas, R. Nicolson, K.M. Hayashi, A.W. Toga, and P.M. Thompson, *Brain structural mapping using a novel hybrid implicit/explicit framework based on the level-set method*, NeuroImage **24** (2005), no. 3, 910–927.
- [14] N.A. Lord, J. Ho, B.C. Vemuri, and S. Eisenschenk, *Simultaneous registration and parcellation of bilateral hippocampal surface pairs for local asymmetry quantification*, Medical Imaging, IEEE Transactions on **26** (2007), no. 4, 471–478.
- [15] L.M. Lui, K.C. Lam, S.-T. Yau, and X. Gu, *Teichmüller extremal mapping and its applications to landmark matching registration*, arXiv preprint arXiv:1211.2569 (2012).
- [16] L.M. Lui, S. Thiruvankadam, Y. Wang, T.F. Chan, and P.M. Thompson, *Optimized conformal parameterization of cortical surfaces using shape based matching of landmark curves*, Medical Image Computing and Computer-Assisted Intervention–MICCAI 2008, Springer, 2008, pp. 494–501.

- [17] L.M. Lui, S. Thiruvankadam, Y. Wang, P.M. Thompson, and T.F. Chan, *Optimized conformal surface registration with shape-based landmark matching*, SIAM Journal on Imaging Sciences **3** (2010), no. 1, 52–78.
- [18] L.M. Lui, Y. Wang, T.F. Chan, and P.M. Thompson, *Landmark constrained genus zero surface conformal mapping and its application to brain mapping research*, Applied numerical mathematics **57** (2007), no. 5, 847–858.
- [19] L.M. Lui, T.W. Wong, X. Gu, P.M. Thompson, T.F. Chan, and S.-T. Yau, *Hippocampal shape registration using beltrami holomorphic flow*, Medical Image Computing and Computer Assisted Intervention (MICCAI), Part II. LNCS, vol. 6362, 2010, pp. 323–330.
- [20] L.M. Lui, T.W. Wong, W. Zeng, X. Gu, P.M. Thompson, T.F. Chan, and S.-T. Yau, *Optimization of surface registrations using beltrami holomorphic flow*, Journal of Scientific Computing **50** (2012), no. 3, 557–585.
- [21] O. Lyttelton, M. Boucher, S. Robbins, and A. Evans, *An unbiased iterative group registration template for cortical surface analysis*, Neuroimage **34** (2007), no. 4, 1535–1544.
- [22] J.B.A. Maintz and M.A. Viergever, *An overview of medical image registration methods*, UU-CS (1998), no. 1998-22.
- [23] L.F. Marcus, *Traditional morphometrics*, Proceedings of the Michigan morphometrics workshop, vol. 2, University of Michigan Museum of Zoology, Ann Arbor, 1990, pp. 77–122.
- [24] M. Reuter, F.-E. Wolter, and N. Peinecke, *Laplace–beltrami spectra as “shape-dna” of surfaces and solids*, Computer-Aided Design **38** (2006), no. 4, 342–366.
- [25] F.J. Rohlf and L.F. Marcus, *A revolution morphometrics*, Trends in Ecology & Evolution **8** (1993), no. 4, 129–132.

- [26] Y. Wang, L.M. Lui, T.F. Chan, and P.M. Thompson, *Optimization of brain conformal mapping with landmarks*, Medical Image Computing and Computer-Assisted Intervention–MICCAI 2005, Springer, 2005, pp. 675–683.
- [27] Y. Wang, L.M. Lui, X. Gu, K.M. Hayashi, T.F. Chan, A.W. Toga, P.M. Thompson, and S.-T. Yau, *Brain surface conformal parameterization using riemann surface structure*, Medical Imaging, IEEE Transactions on **26** (2007), no. 6, 853–865.
- [28] M. Webster and H.D. Sheets, *A practical introduction to landmark-based geometric morphometrics*, Paleontol Soc Papers **16** (2010), 163–188.
- [29] M.L. Zelditch, D.L. Swiderski, and H.D. Sheets, *Geometric morphometrics for biologists: a primer*, Academic Press, 2012.
- [30] W. Zeng and X. Gu, *Registration for 3d surfaces with large deformations using quasi-conformal curvature flow*, Computer Vision and Pattern Recognition (CVPR), 2011 IEEE Conference on, IEEE, 2011, pp. 2457–2464.
- [31] W. Zeng, L.M. Lui, F. Luo, T.F. Chan, S.-T. Yau, and D. Gu, *Computing quasiconformal maps using an auxiliary metric and discrete curvature flow*, Numerische Mathematik **121** (2012), no. 4, 671–703.
- [32] M. Zhang, F. Li, Y. He, S. Lin, D. Wang, and L.M. Lui, *Registration of brainstem surfaces in adolescent idiopathic scoliosis using discrete ricci flow*, Medical Image Computing and Computer-Assisted Intervention–MICCAI 2012, Springer, 2012, pp. 146–154.